sustainability

MDPI

Article

A Data-Driven Stochastic Multi-Objective Energy Management System for Sustainable Interconnected Microgrids, Integrating LSTM Forecasts and Hybrid Storage Systems

Ehab Issa El-Sayed [1], Ahmed. A. F. Youssef [2], Salah K. ElSayed [3,*], Ilyes Boulkaibet [2], Faris H. Alotaibi [3] and Ali M. El-Rifaie [2]

[1] Electrical Power Department, Higher Institute of Engineering and Technology—Fifth Settlement, Cairo 11835, Egypt; ehabissa99@gmail.com
[2] College of Engineering and Technology, American University of the Middle East, Egaila 54200, Kuwait; ahmed.youssef@aum.edu.kw (A.A.F.Y.); ilyes.boulkaibet@aum.edu.kw (I.B.); ali.el-rifaie@aum.edu.kw (A.M.E.-R.)
[3] Department of Electrical Engineering, College of Engineering, Taif University, P.O. Box 11099, Taif 21944, Saudi Arabia; f.hamad@tu.edu.sa
* Correspondence: sabdelhamid@tu.edu.sa

Abstract

The research proposes an EMS for grid-connected microgrids which incorporates deep learning predictions, stochastic optimization, and multi-carrier storage systems to optimize cost of operations and greenhouse gas emissions. By jointly reducing operational costs and carbon emissions, the suggested approach will facilitate the transition to sustainable, resilient, low-carbon energy systems. Quick-acting battery storage and slow-reacting hydrogen are used for shaving peaks and balancing energy supply, while decision-making is robustified against the uncertainty associated with renewables through Latin Hypercube Sampling (LHS). The LSTM-based model forecasts 24 h ahead multi-step PV and wind generation outputs. Five algorithms, namely, GA, PSO, GWO, NSGA-II, and the Hippopotamus optimizer (HO), are evaluated for two different microgrid structures (MG1, MG2), using hypervolume metrics and a Wilcoxon rank-sum test conducted on 30 independent runs. The findings indicated that HO provides the best spread and dispersion of the Pareto frontier, along with highest hypervolume, being statistically similar to PSO ($p > 0.05$), while proving significantly superior to GA and NSGA-II, which get stuck within a highly inefficient region. GWO is overestimated in terms of Pareto convergence, since it is possible at one certain point only. This is impossible in real life, as proven through a peer-to-peer trading counterfactual study. An EMS is capable of allocating renewable excesses into batteries or hydrogen storage and optimizing the profits from grid trading during the 24 h periods. The findings prove HO and PSO algorithms to be reliable energy management solvers for microgrids.

Keywords: microgrid energy management; multi-objective optimization; Hippopotamus optimizer; hydrogen storage; Latin Hypercube Sampling; LSTM forecasting; carbon emission reduction

Check for updates

Academic Editor: Carlos Vargas-Salgado

Received: 22 September 2026
Revised: 19 October 2026
Accepted: 22 October 2026
Published: 25 October 2026

Copyright: © 2026 by the authors. Licensee MDPI, Basel, Switzerland. This article is an open access article distributed under the terms and conditions of the Creative Commons Attribution (CC BY) license.

1. Introduction

In order to lower costs and emissions while increasing dependability, microgrid energy management has recently been presented as a multi-objective, uncertainty-aware optimization problem that coordinates renewables, storage, demand response, and intelligent forecasting. Growing demand, environmental concerns, and rapid deployment of

distributed renewable energy are driving the shift from centralized power systems to decentralized microgrids. In order to combine economic, technological, and environmental goals in the face of unpredictability, microgrids that integrate solar panels, wind turbines, controlled generators, and storage require advanced energy management systems (EMSs) [1,2]. In an effort to reduce operational costs and emissions, as well as occasional losses and voltage variations, numerous studies model grid-connected or islanded microgrids using hybrid sources, such as PV, wind, fuel cells, microturbines, diesel generators, and battery energy storage systems [3,4]. In order to solve non-linear, constrained dispatch issues and outperform traditional methods in terms of cost and emission reduction, advanced metaheuristics, including quantum particle swarm optimization, the lightning search algorithm, and several hybrid optimizers, have been presented [1,4–6]. Stochastic and resilient EMS formulations, such as interval optimization, two-stage stochastic optimization using Monte Carlo scenarios, and information-gap decision theory, have been driven by uncertainty in renewable generation, loads, and prices [7–9]. Coordinated load shifting and state-of-charge management can save costs and improve reliability, as these strategies frequently co-optimize demand response and battery operation [8,9].

In order to change load profiles and incorporate flexible resources like EVs, EV charging stations, and aggregators, demand response and prosumer involvement are becoming more and more integrated into EMS models [10–12]. Time-of-use tariffs and well-designed incentives can significantly lower generation costs and peak demand, according to bi-level and DSM-based formulations [12,13]. Multi-year stochastic models incorporate distributed generators, battery storage, and demand response at the planning level to maximize renewable penetration and reduce long-term costs, losses, and voltage variation [14–16]. Coordinated PV, wind, and BESS siting with DR and network reconfiguration can significantly reduce system costs and losses while increasing renewable utilization, according to past studies [14,15]. These optimization frameworks are enhanced by sophisticated control and forecasting methods. Support vector regression and other machine learning models greatly increase the accuracy of PV and wind power forecasts, which immediately lowers operational costs and improves supply–demand balance in grid-connected microgrids [2,17]. When battery energy storage, multi-microgrids, and renewable clusters are coordinated under market interactions and uncertainty, robust EMS designs also emerge in long-term planning and game-theoretic contexts [16]. In general, the current research presents the microgrid EMS as an integrated optimization and control problem that, in order to achieve economical, low-emission, and dependable operation, must simultaneously take into account renewable intermittency, storage behavior, demand flexibility, and market processes [16–22].

2. Literature Review

In efforts to integrate a significant share of distributed renewable energy while preserving reliability, economic efficiency, and environmental sustainability, microgrids have become a crucial enabler. Effective energy management systems (EMSs) are essential for coordinating photovoltaic (PV) arrays, wind turbines, conventional units, and storage devices under unpredictable operating conditions and fluctuating electricity costs, according to recent research. In a broad body of work, microgrid scheduling is formulated as a multi-objective optimization problem that typically minimizes operating costs and greenhouse gas emissions, occasionally incorporating additional technical indicators such as losses, voltage quality, and reliability. The nonlinear, uncertain, and multi-timescale aspects of microgrid operation are being addressed by combining advanced meta-heuristic algorithms, stochastic modeling, and learning-based forecasting or control.

Multi-objective cost–emission optimization in grid-connected microgrids with renewable energy and battery storage is the subject of numerous recent studies. Quantum particle swarm optimization (QPSO) for a grid-connected EMS is one line of work that specifically aims to reduce carbon emissions and operating costs simultaneously in microgrids with PV, wind, conventional units, and batteries [1]. By overcoming premature convergence and solution stagnation, which frequently constrain conventional metaheuristics, the quantum-inspired mechanics enable quantifiable cost and CO_2 savings across multiple configurations. Similar to this, other studies develop tri-objective EMS models that jointly minimize CO_2 emissions, network energy losses, and operating costs in AC microgrids with distributed PV generators. These models are solved using modified JAYA algorithms and benchmarked against GA, PSO, and other optimizers [23]. Though they frequently only take into account one storage technology and concentrate on a specific microgrid configuration, these studies usually come to the conclusion that correctly calibrated meta-heuristics can offer significant percentage reductions in cost and emissions when compared with baseline techniques. Several studies combine system sizing with an EMS to capture long-term techno-economic and environmental trade-offs, going beyond simple operational scheduling. Over a multidecade project horizon, a joint mixed-integer linear programming framework has been suggested that simultaneously optimizes the sizing and hourly operation of PV and battery systems, both with and without grid connection [24]. This method demonstrates how limitations like grid subscription power have a substantial impact on both cost and local renewable utilization, using Pareto fronts for the levelized cost of energy and life cycle emissions. Other research on hybrid solar–wind microgrids with diesel and biomass backup employs multi-algorithm comparisons, such as PSO, GA, GWO, and hybrid GWO–Cuckoo Search, to find cost-optimal sizing solutions, with a focus on component counts, robustness, and levelized cost of energy as outcomes of interest [25]. The significance of algorithm selection for attaining low annual cost and high renewable fractions in grid-connected hybrids is highlighted by related studies that statistically benchmark families of more recent metaheuristics, such as Hunger Games Search, Kepler, or Fire Hawk optimizers for hybrid PV–wind–battery–supercapacitor systems [26].

Simultaneously, stochastic and uncertainty-aware EMS formulations are receiving more attention. One line of inquiry creates stochastic scheduling models for microgrids that specifically account for demand unpredictability and renewable energy sources, occasionally in conjunction with demand response and mobile storage. For instance, in microgrids with static and mobile storage, a stochastic energy management system based on the two-point estimate method and an improved multi-objective grey wolf optimizer concurrently increases renewable hosting capacity and reduces both operational and emission costs [27,28]. This method quantifies how stochastic issue formulations raise costs while enhancing resilience and demonstrates how explicitly addressing dynamic mobile storage and uncertainties modifies optimal location and sizing decisions. An innovative optimization technique based on mountaineering teams is used in another line of work to offer an uncertainty-aware EMS that integrates mobile storage, green certificate markets, and electric vehicle and e-bike charging [29]. Here, compared to deterministic situations, stochastic scenarios change the trade-offs between operational cost, emissions, and certificate income, demonstrating how adding variability can lower projected profit while producing more reliable scheduling choices. Deterministic microgrid formulations frequently offer greater nominal cost savings when compared to these works, but they do not quantify the risk of forecast errors. Storage modeling and dispatch procedures under uncertainty are the subject of a related strand. In a microgrid with PV, wind, batteries, and diesel units, recent research suggests multifunctional battery storage that handles both supply–demand balancing and energy arbitrage [30]. These studies use Latin Hypercube Sampling (LHS) to capture wind and

solar uncertainties and create multi-objective problems that minimize total microgrid cost, harmful gas emissions, and power mismatch. These issues are handled using algorithms like Moth Flame Optimization and hybrid Firefly–PSO. Similar to this, slime mold optimizers are used in transactive EMS strategies for grid-connected microgrids with renewable energy sources to co-optimize scheduling and battery storage utilization. This demonstrates how adding storage changes the solution from pure tariff arbitrage to deeper cost and emission reductions by utilizing dynamic charging and discharging [31]. Although these frameworks usually optimize heuristically rather than via multi-objective metaheuristics, standalone DC microgrids with PV, fuel cells, and batteries have also been studied with rule-based EMSs that control PV derating and fuel cell power as functions of battery state of charge to mitigate deep cycling and hydrogen consumption over long horizons [32,33].

Beyond single-carrier storage, hybrid and multi-carrier storage architectures are increasingly being investigated. Several contributions explore hybrid hydrogen–battery systems, where electrolyzers, fuel cells, and hydrogen tanks complement batteries to provide seasonal or long-duration storage. One recent framework for long-term microgrid management with hybrid hydrogen–battery storage develops a semi-empirical hydrogen model and a prediction-free online convex optimization scheme to track annual hydrogen state-of-charge references, reducing both operational costs and loss-of-load probability relative to existing online methods [34]. Other work models PV–battery–hydrogen microgrids for cost and carbon reduction, showing, via simulation, that combining battery and hydrogen storage leads to notable reductions in carbon emissions and total energy cost compared with single-storage configurations [35,36]. In addition, multi-carrier microgrids that couple electrical, thermal, and hydrogen loads with various storage technologies are managed via scenario-based stochastic EMS, demonstrating that sector coupling and cross-vector storage can further reduce costs and emissions beyond pure electrical microgrids [37]. Compared with these studies, many cost–emission EMS works still employ only a single battery storage unit, leaving a gap in coordinated optimization between fast and long-term storages. Akarnae et al. [38], more recently, have proposed a BSSA-based EMS for AC microgrids with joint optimization of generation-side dispatch (PV, WTS, BSS, and grid) and scheduling of appliances on the consumption side at 15 min intervals, resulting in a 33.34% decrease in costs and PAR value of 9.62 compared to PSO and GA; but still, the strategy is deterministic, single-objective (weighted sum), and does not address the issues of renewable/prices uncertainty, peer-to-peer transactions, and battery–hydrogen combination systems.

The recent literature also emphasizes improved forecasting and learning-based EMSs. LSTM deep learning has been applied to forecast PV and wind generation, market prices, and loads for improved economic dispatch in grid-connected hybrid PV–wind microgrids under an MILP-based EMS, demonstrating that better multi-step forecasts directly enhance revenue and inform battery degradation-aware scheduling [39]. Spatiotemporal forecasting models that exploit meteorological features and multi-timescale optimization have likewise been shown to improve solar prediction accuracy, reduce energy costs, and enhance voltage stability versus model predictive control and deep reinforcement learning baselines [40]. At the control layer, deep reinforcement learning has been used to coordinate multiple sources and dual-battery chemistries in off-grid microgrids, framing operation as a multi-objective problem over life-cycle cost, LCOE, and emissions, and demonstrating that a DQN-based EMS can outperform rule-based policies and even some meta-heuristic-optimized static dispatch in terms of cost and battery degradation [41]. Reinforcement learning can internalize multiple objectives, such as battery degradation and renewable uncertainty, according to recent reviews of adaptive multi-objective optimization with deep reinforcement learning. However, many of these studies still rely on precise forecasts and do not always benchmark against robust multi-objective metaheuristics [42]. The expansion from individual

microgrids to coalitions or communities is another developing trend. For coalitions of interconnected smart microgrids, multi-objective stochastic models that integrate renewable energy, electric vehicles, and demand response while reducing costs and emissions under uncertainty have been presented [43] These simulations demonstrate that coordinated operation of many microgrids results in additional large cost and emission reductions compared to independent operation by integrating ε constraint approaches with Benders decomposition. Simultaneously, stochastic hybrid wind–PV–battery projects are assessed from an investment standpoint using response surface methodology, experiment design, and desirability functions to minimize financial risk and maximize expected net present value, highlighting the importance of economic uncertainty in long-term planning alongside technical variability [44]. In contrast to this literature, a microgrid EMS that integrates multiple carrier storage (long-term hydrogen and fast BESS), explicit stochastic scenario generation (e.g., through Latin Hypercube Sampling), deep learning-based multi-step forecasts for wind and PV, and systematic benchmarking of multiple metaheuristics over multiple microgrid topologies simultaneously fills several gaps. Current research frequently treats storage as a single battery system without coordinated hydrogen loops, or it optimizes cost and emissions using one or two metaheuristics in a single architecture. Others concentrate on hydrogen–battery coordination, but they either do not systematically assess different algorithms on Pareto front quality or utilize prediction-free convex optimization with limited forecasting power. Similarly, a lot of EMS frameworks based on LSTM or RL enhance forecasting or control separately but do not incorporate detailed stochastic scenario creation and multi-carrier storage within a single, multi-objective optimization architecture. An EMS that shows, across two different microgrid configurations, both improved Pareto front diversity and superior compromise solutions on cost and emissions with a particular algorithm can be positioned as a comprehensive advancement integrating and extending several of these recent research directions by contrasting these patterns of contribution and reported conclusions—such as percentage cost and CO_2 reductions, improvements in hosting capacity or voltage stability, or qualitative claims about robustness. The novelty in this work comes from integration at the systems level. Even though LSTM forecasting, LHS-based scenarios, hydrogen–battery storage systems, and the Hippopotamus Optimizer (HO) algorithm have been explored in the literature, the co-design of the above, where the stochastic scenarios become input to a dispatch problem using a two-storage (fast BESS and long duration H2) approach in five metaheuristic algorithms for two microgrids. Figure 1 illustrates the layout of the model. The technical and environmental parameters utilized for modeling the microgrids (MG1 and MG2) in this study were derived from established industry standards and the recent literature [45–57].

The contributions of this paper are as follows: (i) a multi-carrier energy storage framework integrating battery systems with hydrogen storage loops is developed to optimize peak-shaving and energy stabilization; (ii) a Latin Hypercube Sampling (LHS)-based stochastic scenario generation method is adopted to hedge operational dispatch decisions against renewable energy uncertainties; (iii) a multi-objective optimization model is formulated to simultaneously minimize operational costs and CO_2 emissions over a 24 h horizon; (iv) five meta-heuristic algorithms, namely, GA, PSO, GWO, NSGA-II, and HO, are benchmarked to identify the optimal solver for different operational priorities; (v) the proposed framework is validated across two distinct microgrid topologies (MG1 and MG2) to demonstrate its structural adaptability and scalability; and (vi) an LSTM-based deep learning model is implemented for multi-step ahead recursive forecasting of photovoltaic and wind turbine power profiles over a rolling 24 h horizon. The paper is organized as follows. Section 2 presents a literature review. Section 3 describes the optimization and

scenario generation methodology. Section 4 details the forecasting framework and discusses the results, and Section 5 concludes the paper.

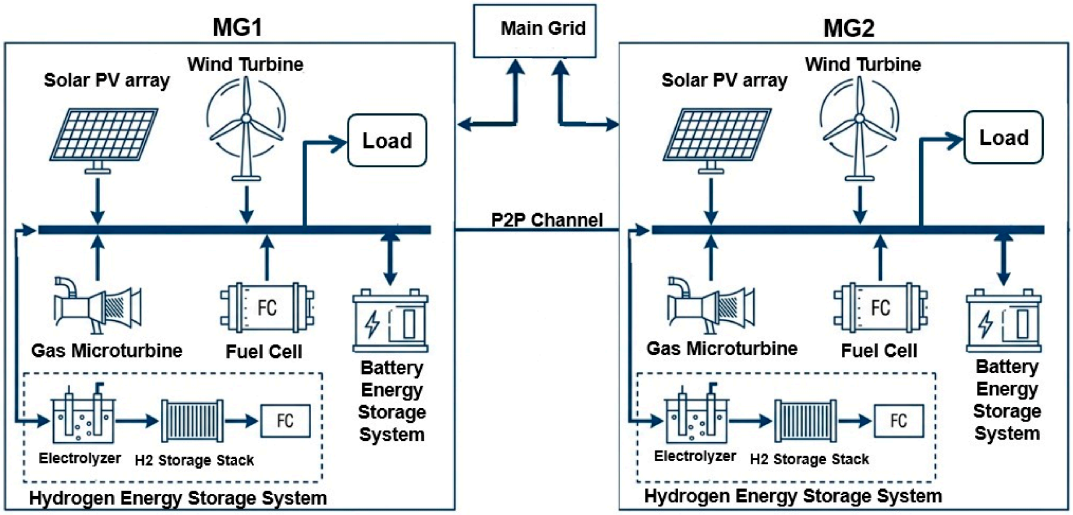


Figure 1. Schematic diagram of the interconnected dual-microgrid architecture.

3. Methodology

This section presents the mathematical framework and the core algorithmic structure of the multi-objective energy management system (EMS) designed for coordinated microgrids. The formulation handles deterministic and stochastic profiles for two independent microgrid test topologies MG1 and MG2 over a scheduling horizon T = 24.

3.1. Microgrid Architecture and Decision Variables

Each microgrid consists of a combination of conventional distributed generators, renewable energy sources, and energy storage systems. The dispatch portfolio optimizes eight distinct profiles over hours, forming a continuous optimization space with decision vector X of size 8T.

$$X = \left[P_{mt},\ P_{fc}, P_{dg}, P_{bat}, P_{grid}, P_{el}, P_{h2}, P_{tr}\right] \quad (1)$$

where the components for each time step T = 1, ..., 24. P_{mt}: microturbine generation dispatch vector, P_{fc}: fuel cell unit output vector, P_{dg}: diesel generator dispatch profile, P_{bat}: battery storage charge/discharge profile, P_{grid}: main utility grid power exchange vector, positive = import, negative = export, P_{el}: hydrogen electrolyzer power consumption profile, P_{h2}: hydrogen fuel cell storage generation profile, P_{tr}: peer to peer microgrid energy trading profile.

3.2. Machine Learning-Based Forecasting Engine

To eliminate the unrealistic assumption of perfect foresight frequently observed in deterministic energy management models, this study establishes a robust data-driven predictive framework using deep recurrent neural networks. With their non-linear dynamics and intricate temporal connections, solar photovoltaic PV generation and wind turbine WT power are heavily reliant on changing weather. A long short-term memory (LSTM) architecture is used to calculate look-ahead generation profiles across a 24 h forecasting horizon in order to identify these trends. These data-driven predictions serve as the absolute baseline trajectory for the downstream microgrid optimization engine [58–60].

The construction of a typical LSTM unit is seen in Figure 2, where c_k represents the unit memory at time t equals k

$$c_k = f_k.c_{k-1} + i_k.\tilde{c}_k \quad (2)$$

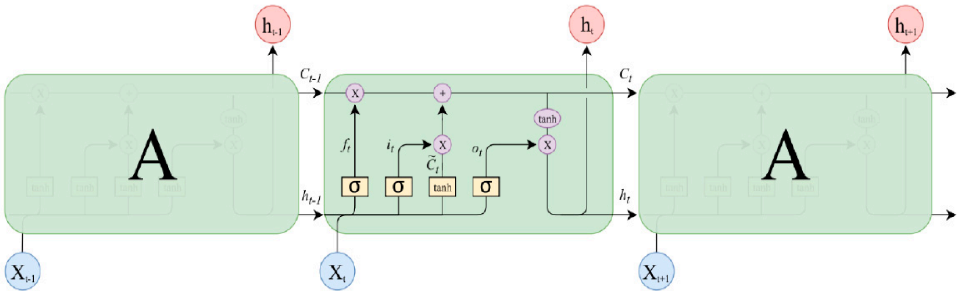


Figure 2. LSTM architecture.

The three types of gates that the LSTM unit uses to calculate the effects of cell memory on node output, the forgetting rate of cell memory upon current input, and the percentage of current cell memory merging into old cell memory are input gate I, forget gate F, and output gate O. At time k, an LSTM unit makes a forward pass in the manner described below:

$$\begin{gathered} f_k = \sigma_g(w_f x_k + U_f h_{k-1} + b_f) \\ i_k = \sigma_g(w_i x_k + U_i h_{k-1} + b_i) \\ o_k = \sigma_g(w_o x_k + U_o h_{k-1} + b_o) \\ c_k = f_k \circ c_{k-1} + i_k \circ \sigma_c(w_c x_k + U_c h_{k-1} + b_c) \\ h_k = o_k \circ \sigma_h(c_k) \end{gathered} \quad (3)$$

where x_k and h_k are the unit input and referring output at time k, consequently; c_k indicates the hidden cell memory; W, U, and b are weight matrices and bias vectors to be learned during training; o signifies the element-wise product of the vectors. The activation vectors of the input gate, forget gate, and output gate are denoted by the symbols f_k, i_k, and o_k, respectively, while σ_g, σ_h,σ_c are the associated activation functions; more precisely, σ_g is a logistic sigmoid function, while σ_c and σ_h are both hyperbolic tangent functions.

3.3. Stochastic Scenario Generation

To hedge against the intermittent behaviors of solar photovoltaics (PV) and wind turbine (WT) output, Latin Hypercube Sampling (LHS) generates a scenario matrix. The stochastic representation used in this study concentrated specifically on the renewable-generation uncertainties, due to their predominance in the studied microgrids. Let $P_{PV,0}(t)$ and $P_{WT,0}(t)$ be the base forecast values at hour t. Scenarios are generated via

$$P_{PV}(t,s) = \max\left(0, P_{PV,0}(t)\cdot(1 + \sigma_{pv}.\zeta_{pv}(t,s))\right), \qquad \forall t \in T, \forall s \in N_{sc} \quad (4)$$

$$P_{WT}(t,s) = \max\left(0, P_{WT,0}(t)\cdot(1 + \sigma_{WT}.\zeta_{WT}(t,s))\right), \qquad \forall t \in T, \forall s \in N_{sc} \quad (5)$$

where the localized forecast error represents uncertainty deviation ($\sigma = 20\%$). Localized forecast error uncertainty deviation for Equations (4) and (5) is intentionally chosen to be a conservative upper bound relative to the forecast errors of the LSTM model, ζ values are standard normal variables sampled via LHS distributions, and $N_{sc} = 10$ is the complete index of simulated scenarios. Each scenario s is assigned equal probability $P_s = 1/N_{sc}$ [61,62].

3.4. Objective Function Formulations

The framework simultaneously minimizes operational expenditure (f_1) and carbon footprint greenhouse gas indices (f_2).

3.4.1. Economic Operating Cost Mitigation f_1

The operating cost objective function aggregates conventional generation fuel expenditures, battery degradation premiums, and utility grid dynamic tariff payments across scenarios [1]:

$$f_1(X) = \frac{1}{N_{sc}} \sum_{s=1}^{N_{sc}} \sum_{t=1}^{T} \left(C_{gen}(t) + C_{grid}(t,s) \right) \quad (6)$$

$$C_{gen}(t) = P_{mt}(\mathrm{t})\, c_{mt} + P_{fc}(\mathrm{t})\, c_{fc} + P_{dg}(\mathrm{t})\, c_{dg} + P_{bat}(\mathrm{t})\, c_{deg} \quad (7)$$

$$C_{grid}(t,s) = \begin{cases} P_{grid}(t,s) \cdot \gamma_{buy}(t), P_{grid}(t,s) \geq 0 \\ P_{grid}(t,s) \cdot \gamma_{sell}(t), P_{grid}(t,s) < 0 \end{cases} \quad (8)$$

where c_{mt}, c_{fc},c_{dg} represent generation coefficients (0.088, 0.145, and 0.320 \$/kwh). The c_{deg} is the battery degradation factor (0.00012 \$/kwh) and $\gamma_{buy}(t)$, $\gamma_{sell}(\mathrm{t})$ represent utility tariffs.

3.4.2. Environmental Carbon Footprint Index (f_2)

Greenhouse gas calculations aggregate equivalent emissions intensities derived from dispatch operations [34,63]:

$$f_2(X) = \frac{1}{N_{sc}} \sum_{s=1}^{N_{sc}} \sum_{t=1}^{T} \left(P_{mt}(t)\varepsilon_{mt} + P_{fc}(t)\varepsilon_{fc} + P_{dg}(t)\varepsilon_{dg} + \max\left(P_{grid}(t,s), 0\right)\varepsilon_{grid} + P_{h2}(t)\varepsilon_{h2} \right) \quad (9)$$

where ε denotes lifecycle emissions coefficients per generation block ($\varepsilon_{mt} = 0.500$, $\varepsilon_{fc} = 0.410$, $\varepsilon_{dg} = 0.950$, $\varepsilon_{grid} = 0.210$, $\varepsilon_{h2} = 0.015$ Kg CO_2/kwh).

3.4.3. Scalar Aggregate Objective with Carbon Pricing

For single-objective metaheuristic variants (GA, PSO, GWO, and HO), multi-objective problems are converted into single-objective metrics using carbon tax parameters during runtime [64–68]:

$$\text{Minimize} \cdot \mathrm{J} = \cdot f_1(X) + \gamma_{carbon} \cdot f_2(X) + \mathcal{P}(x) \quad (10)$$

where $\gamma_{carbon} = 50$ \$/kgCO_2. For the multi-objective NSGA-II variant, vectors $[f_1(X), f_2(X)]$ are processed natively using Pareto dominance sorting definition:

$$\mathrm{u} \prec \mathrm{v}\ \forall_i \in \{1,2\}: f_i(u) \leq f_i(v) \wedge \exists i \in \{1,2\}: f_i(u) < f_i(v) \quad (11)$$

Solutions mapping directly to the undominated surface boundary are extracted to build the final Pareto comparison logs.

3.5. System Operational Constraints

3.5.1. Power Balance Equality Constraint

At every time step t, the grid exchange variable P_{grid} (t) is computed analytically from the remaining decision variables, enforcing nodal power balance as a hard equality and reducing the search space by T dimensions:

$$P_{grid}(t,s) = P_L(t) + P_{el}(t) - (P_{mt}(t) + P_{fc}(t) + P_{dg}(t) + P_{PV}(t,s) + P_{WT}(t,s) + P_{bat}(t) + P_{h2}(t) + P_{tr}(t)) \quad (12)$$

3.5.2. Physical Device Operation Constraints

Each device must operate within its specified boundaries:

$$\begin{gathered} 0 \le P_{mt}(t) \le P_{mt},max \\ 0 \le P_{fc}(t) \le P_{fc},max \\ 0 \le P_{dg}(t) \le P_{dg},max \\ -P_{bat},max \le P_{bat}(t) \le P_{bat},max \\ -P_{tr},max \le P_{tr}(t) \le P_{tr},max \\ 0 \le P_{el}(t) \le P_{el},max \\ 0 \le P_{h2}(t) \le P_{h2},max \\ \left|P_{grid}(t)\right| \le P_{grid},max \end{gathered} \tag{13}$$

3.6. Energy Storage System Dynamics

3.6.1. Battery State of Charge

Storage profiles update recursively based on charge and discharge states:

The battery SOC evolves through a discrete-time energy balance with asymmetric charge/discharge efficiencies ($\eta_{ch} = \eta_{dis} = 0.95$). The recursive battery state-of-charge equation handles charging ($P_{bat}(t) < 0$) and discharging ($P_{bat}(t) \ge 0$) efficiencies dynamically [34].

$$SOC_{bat}(t) = \begin{cases} SOC_{bat}(t-1) - \frac{P_{bat}(t).\Delta t}{\eta_{dis}}, P_{bat}(t) \ge 0 \\ SOC_{bat}(t-1) - P_{bat}(t) \cdot \eta_{ch}.\Delta t, P_{bat}(t) < 0 \end{cases} SOC_{bat,Min} \le SOC_{bat}(t) \le SOC_{bat,Max}, 20 \text{ kwh} \le SOC_{bat}(t) \le 200 \text{ kwh} \tag{14}$$

3.6.2. Hydrogen Storage State of Charge

The hydrogen system uses the electrolyzer to charge (consume electricity and store hydrogen) and the hydrogen fuel cell to discharge. The tank SOC evolves as [69,70]

$$SOC_{h2}(t) = SOC_{h2}(t-1) + P_{el}(t) \cdot \eta_{el} - \frac{P_{h2}(t)}{\eta_{fc}} \tag{15}$$

$$SOC_{h2,Min} \le SOC_{h2}(t) \le SOC_{h2,Max}, 20 \text{ kwh} \le SOC_{h2}(t) \le 200 \text{ kwh} \tag{16}$$

where $\eta_{el} = 0.7$, $\eta_{fc} = 0.60$.

3.7. Constraint Handling via Exterior Penalty Method

All inequality constraints are enforced through a quadratic exterior penalty augmenting the objective function [71]. The total penalty function is

$$\mathcal{P}(x) = \kappa \cdot [\mathcal{P}_{soc,bat} + \mathcal{P}_{soc,h2} + \mathcal{P}_{grid}], \text{where K} = 106 \tag{17}$$

For any storage device with bounds [SOC_{Min}n, SOCmax], the SOC violation penalty includes a terminal stability term ensuring cyclic energy neutrality:

$$\mathcal{P}_{soc} = \sum_{t=1}^{T} [\max(0, SOC_{Min} - SOC(t))^2 + \max(0, SOC(t) - SOC_{Max})^2] + 50 \cdot \left(SOC(T) - SOC_{(0)} \right)^2 \tag{18}$$

$$\mathcal{P}_{grid} = \sum_t \max\left(0, \left|P_{grid}(t)\right| - P_{grid,max}\right), P_{grid,max} = 100\text{kw} \tag{19}$$

3.8. Metaheuristic Optimization Execution Routine

The optimization pipeline handles constraints using a two-stage approach: advanced decision variable repair mechanisms resolve spatial balance discrepancies before evaluating fitness metrics. The master architecture systematically passes structural configurations to five benchmark metaheuristic variants [63,72–75]. The energy management framework implements five distinct metaheuristic architectures to verify statistical optimization robustness. The explicit positional update equations for each engine are formulated below.

1. Genetic Algorithm (GA): Utilizes single-point crossover operator matrices and uniform random variable boundaries. For parent decision vector X_A, X_B with a chosen random index cp $\in[1, 8T-1]$, the generated offspring vectors follow:

$$\begin{aligned} X_{child1} &= [X_A(1.....cp), X_B(cp+1.....8T)] \\ X_{child2} &= [X_B(1.....cp), X_A(cp+1.....8T)] \end{aligned} \quad (20)$$

Mutated genes are replaced with a probability of 10% using uniform random distributions across the variable search boundaries $[LB_j, UB_j]$.

2. Particle Swarm Optimization (PSO): Particles modify search path trajectories by tracking their historical personal optimal coordinate ($PBest_i$) and the global group leader coordinate ($gBest$). The operational equations are bound by

$$\begin{aligned} V_i(it+1) &= \omega V_i(it) + c_1 r_1 (PBest_i - X_i(it)) + c_2 r_2 (gBest - X_i(it)) \\ (X_i(it+1)) &= X_i(it) + V_i(it+1) \end{aligned} \quad (21)$$

where the inertia weight is configured as $\omega = 0.7$, and the acceleration components are set as $c_1 = c_2 = 1.5$.

3. Grey Wolf Optimizer (GWO): Simulates the tracking behavior of a hunting pack governed by alpha (α), beta (β), and delta (δ) leadership states. Wolf coordinate movements adapt according to

$$\begin{aligned} D_\alpha = |c_1 \cdot \alpha - X_i|, D_\beta = |c_2 \cdot \beta - X_i|, D_\delta = |c_3 \cdot \delta - X_i| \\ X_1 = \alpha - A_1 \cdot D_\alpha, X_2 = \beta - A_2 \cdot D_\beta, X_3 = \delta - A_3 \cdot D_\delta \\ (X_i(it+1)) = (X_1 + X_2 + X_3)/3 \end{aligned} \quad (22)$$

where An and Cn are random vectors scaled by linearly decreasing exploration parameter $\alpha = 2 - it \cdot \left(\frac{2}{Maxiter}\right)$.

4. Hippopotamus Optimization (HO): Position dynamics replicate the swimming and evasion habits of hippopotamuses in a river. Positions are computed using adaptive distance scaling metrics:

$$\begin{aligned} D &= |B \cdot Best - X_i(it)| \\ X_{new} &= Best - A \cdot D \end{aligned} \quad (23)$$

where A = $2r_1 - 1$ *and* $B = 2r_2$ represent dynamic random search bounds (r_1,$r_2 \in [0, 1]$). If an additional exploration condition satisfies a rondom criteria threshold (rand < 0.5), the position shifts against a rondomly drawn individual index H_{ippo}

$$X_{new} = X_{new} + rand \cdot (X_{randHippo} - X_i(it)) \quad (24)$$

5. Non-dominated Sorting Genetic Algorithm II (NSGA-II): Evaluates multi-objective spaces natively without requiring scalar penalty parameter tuning. To ensure uniform diversity on the frontier border, the technique employs a crowding distance operator and computes Pareto Dominance matrices. The crowding metric for any candidate solution point across objective axes m ∈{1,2} is defined by:

$$crowd(i) = \sum_{m=1}^{2} \frac{f_m(i+1) - f_m(i-1)}{f_m^{max} - f_m^{min}} \quad (25)$$

3.9. Performance Evaluation Metrics

After optimization, the Pareto-optimal set P^* is extracted from the final population X^* by identifying all non-dominated solutions:

$$P^* = \{x \in X^* | \nexists x' \prec x\} \quad (26)$$

3.9.1. Hypervolume Indicator

The volume of objective space dominated by the Pareto front in relation to a reference point r is measured by the hypervolume indicator HV [66]. Objectives are first normalized to $[0, 1]$:

$$f_m(x)' = \frac{f_m(x) - f_m^{min}}{f_m^{max} - f_m^{min} + \varepsilon} \; HV(P^*, r) = \lambda\left(\bigcup_{x \epsilon P^*} [f'(x), r]\right) \quad (27)$$

where $\lambda(\cdot)$ denotes the Lebesgue measure of the dominated hypervolume. Higher HV values indicate better Pareto front quality in terms of both convergence and diversity.

3.9.2. Statistical Robustness

Each algorithm is executed across multiple independent trials. Box plots and Wilcoxon rank-sum tests ($\alpha = 0.05$) assess whether performance differences are statistically significant. Convergence curves are recorded for both MG1 and MG2 to assess optimization stability.

4. Results and Discussion

Performance evaluations for the recommended energy management system (EMS) in both microgrids (MG1 and MG2) are described in this section. Five different metaheuristic algorithms have been considered for solving the EMS optimization problem. These include the Hippopotamus Optimization algorithm (HO), Non-dominated Sorting Genetic Algorithm II (NSGA-II), Grey Wolf Optimizer (GWO), Particle Swarm Optimization (PSO), and Genetic Algorithm (GA). The unpredictable nature of renewable generation necessitated that the optimization problem be solved with the goal of minimizing carbon emissions and operating costs simultaneously. Before feeding the simulated data into machine learning models, it is necessary to properly preprocess the data, using the modeling technique covered in the preceding section. Any machine learning project must begin with data collecting, which also happens to be the initial stage in the data preparation process. Importing the libraries required for machine learning projects, such as NumPy, panda, matplotlib, and seaborn, is the next step. A library is a set of functions that may be called and used by an algorithm. Loading the data that the machine learning algorithm will use is the next crucial step. This is the most important preprocessing step for machine learning. Next, it is time to assess the information and search for any missing values. Lastly, the dataset is divided into sets for training, evaluation, and validation, after which the data preparation stages come to an end. One specific approach is to take the datasets and divide them into 30% for testing and 70% for training, at random. These ratios are commonly used in machine learning to choose the training and test datasets. The LSTM network consists of a single one-LSTM layer between the input and output layers. The LSTM is trained for 50 epochs, with a 16-batch size, 50 hidden units and a linear dense projection head and a 0.2 dropout. Figures 3 and 4 show the performance of actual power versus the predicted power of PV and wind. Also, Figures 5 and 6 show the performance of forecasting error distribution of PV and wind. The proposed single-layer LSTM forecasting engine achieves high tracking fidelity $R^2 = 0.9772, 0.8802$ for PV and wind, respectively, with minimum residual variances over a 24 h look-ahead horizon.

4.1. Optimization Performance of EMS Algorithms

The performance of the proposed EMS architecture for MG1 and MG2 was evaluated under 24 h operating schedules. Pareto-optimal solutions that show the trade-off between cost and emissions are obtained by running the algorithms, as illustrated in the figure. NSGA-II and HO converged to produce stable Pareto fronts with superior distribution compared to GA, PSO, and GWO. In fact, their balanced exploration and exploitation abilities enable them to perform better. As seen from the obtained Pareto fronts in the

figure, obtaining lower emissions incurs higher operating costs, as the participation of diesel generators decreases with augmented renewable/storage utilization. On the other hand, there is increased carbon emission if operating costs are capped.

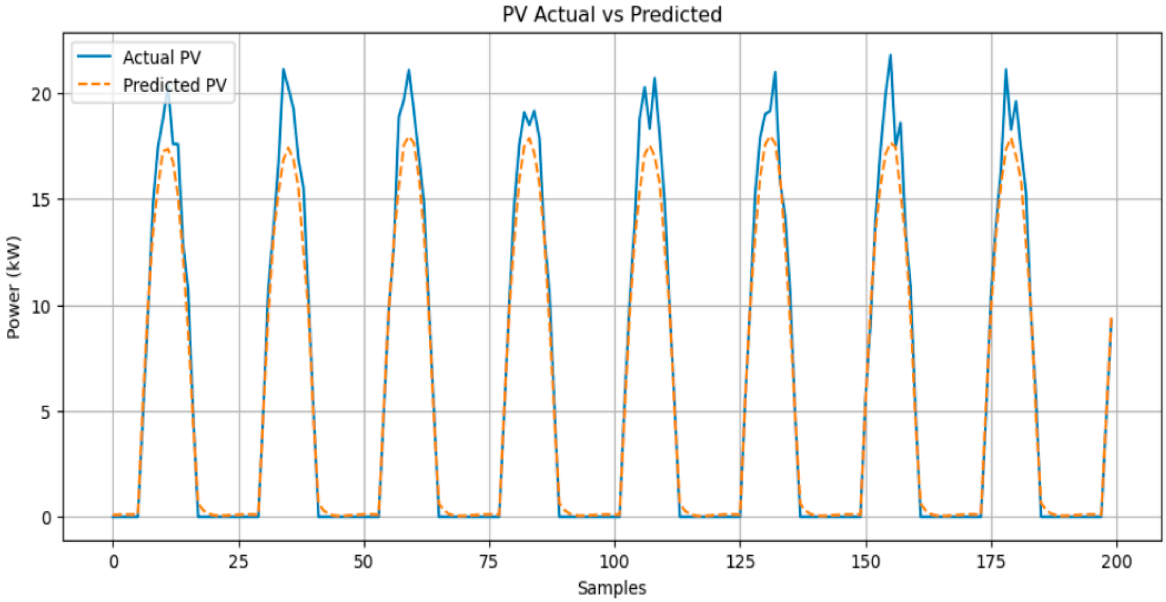


Figure 3. The plot showing actual vs. predicted photovoltaic (PV) power.

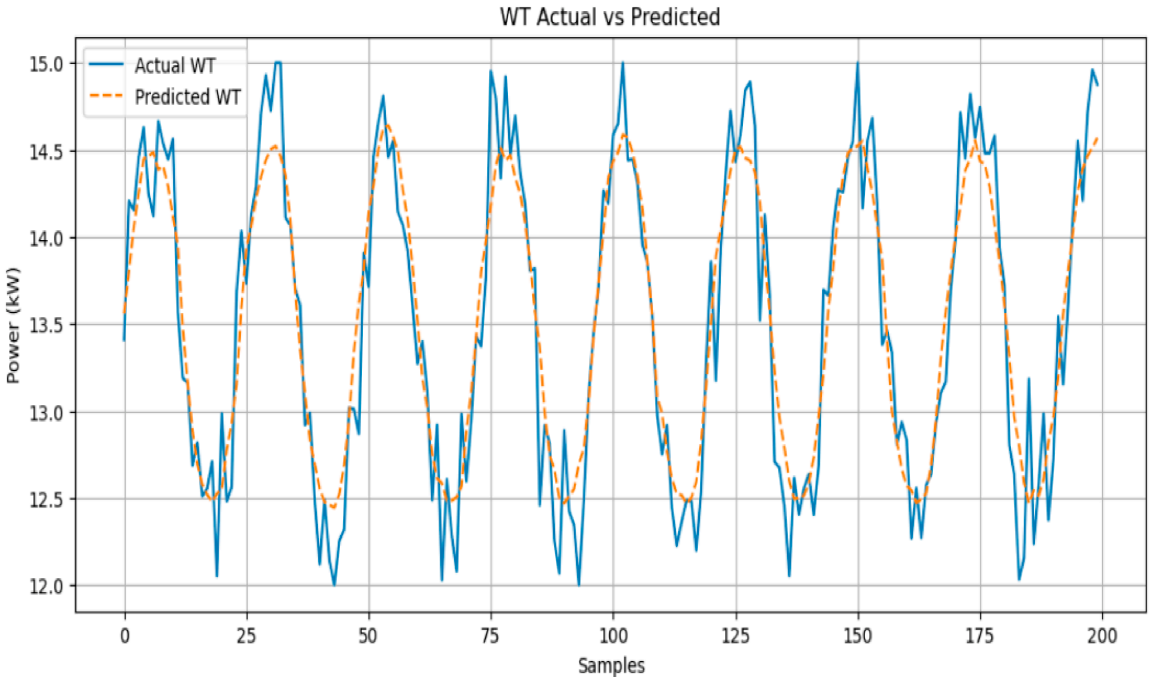


Figure 4. The plot showing actual vs. predicted wind turbine (WT) power.

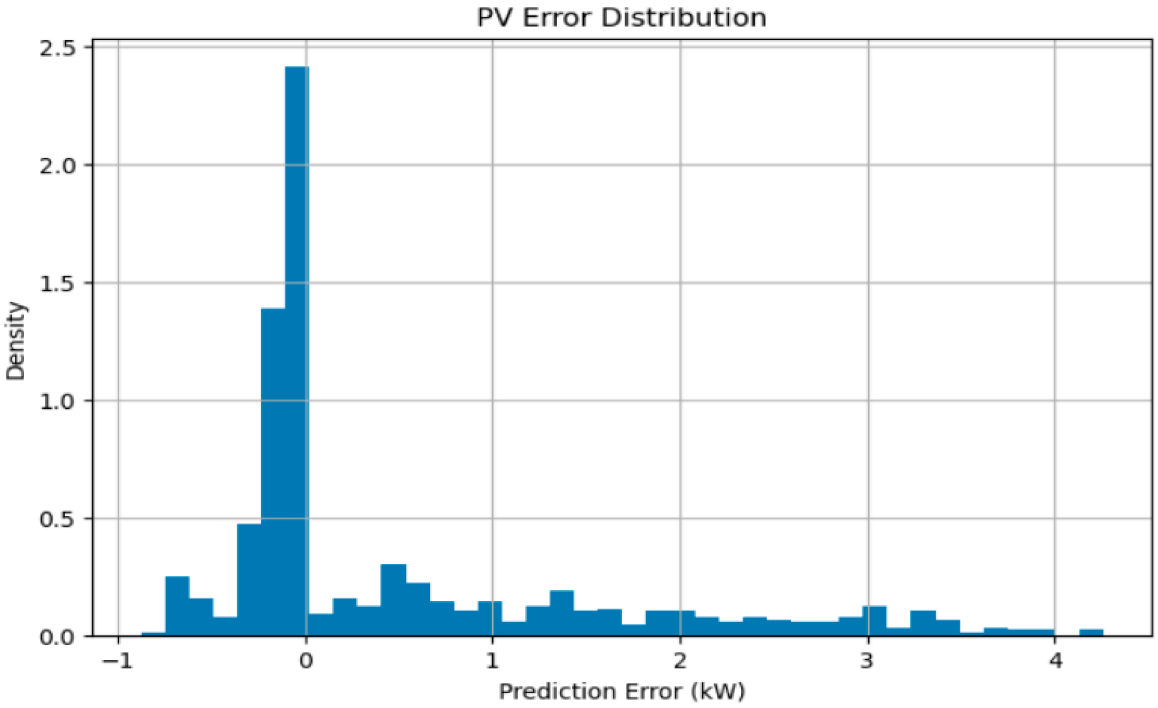


Figure 5. The histogram for the PV forecasting error distribution.

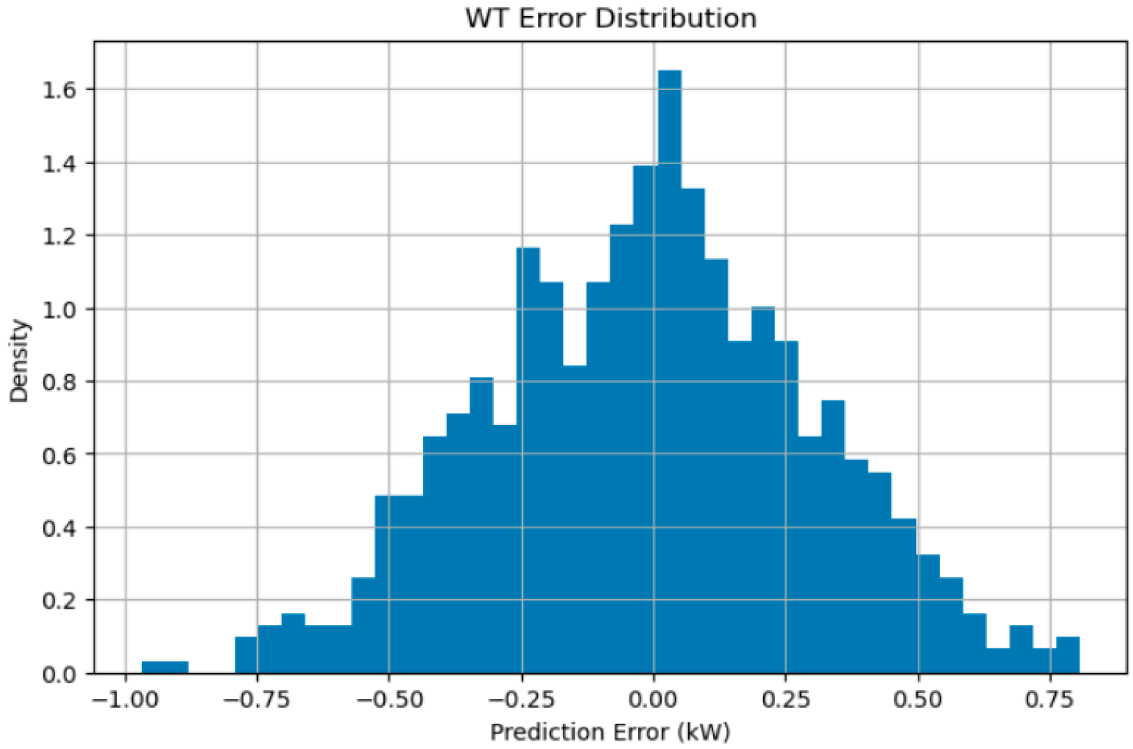


Figure 6. The histogram for the WT forecasting error distribution.

4.2. Pareto Front Analysis

The trade-off between total operating cost and CO_2 emissions is shown by the Pareto fronts produced for MG1 and MG2.

Figures 7 and 8 display the multi-objective Pareto-optimal fronts for Microgrid 1 (MG1) and Microgrid (MG2). Because it can maintain population variety and provide a well-distributed, continuous trade-off curve throughout the entire solution space, Hippopotamus

Optimization (HO) is the best method. In contrast, early convergence causes the Grey Wolf Optimizer (GWO) to collapse into a single-point extreme solution in the negative-cost area (40$). However, unlike HO, which effectively navigates the complicated search space where traditional algorithms like NSGA-II fail to converge, GWO fails as a multi-objective optimizer, since it offers no other compromise alternatives. Figures 9 and 10 illustrate the conflicting multi-objective trade-offs between operational cost and CO_2 emissions for MG1 and MG2.

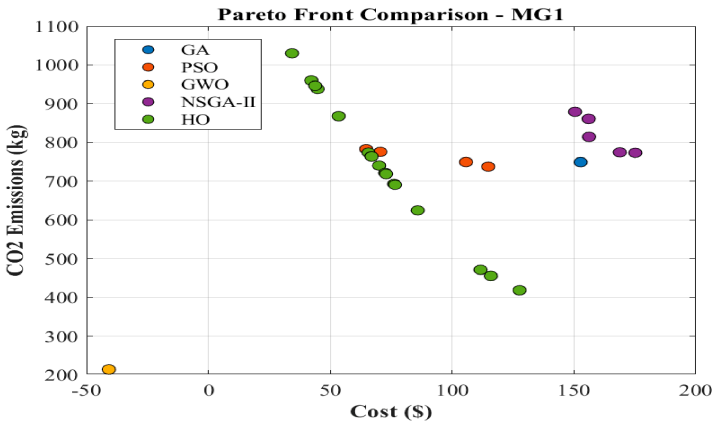


Figure 7. Pareto-optimal front for operating cost and CO_2 emissions in Microgrid MG1.

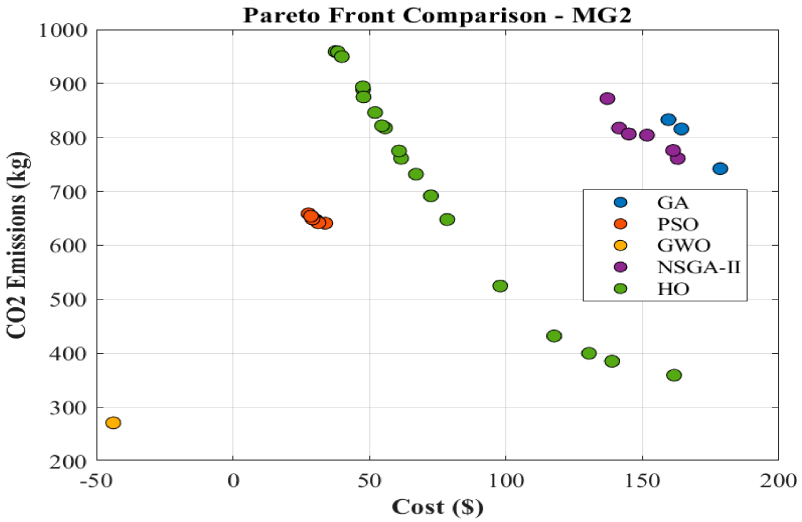


Figure 8. Pareto-optimal front for operating cost and CO_2 emissions in Microgrid MG2.

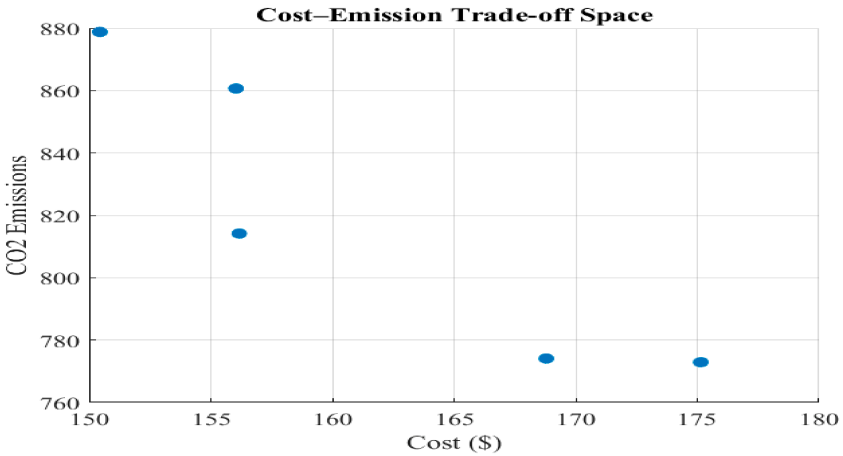


Figure 9. Cost–emission trade-off space for Microgrid 1.

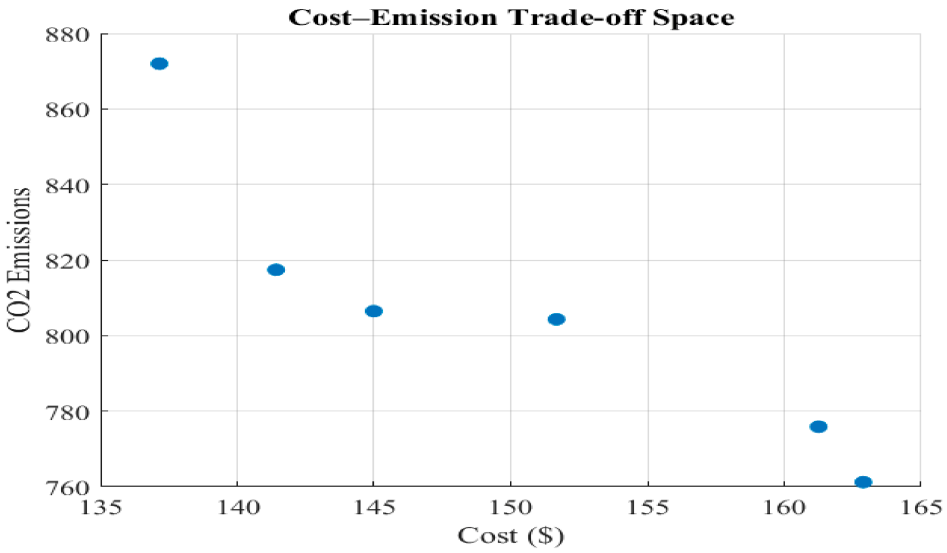


Figure 10. The cost–emission trade-off space for Microgrid 2 illustrates the sub-optimal region where traditional algorithms fall; plots of the localized cost–emission trade-off space for MG1 and MG2 reveal a clearly hostile relationship. MG1's running costs increase from \$150.5 to \$175.2 when CO_2 emissions are lowered from 880 kg to 773 kg. Similarly, MG2 exhibits a local trade-off barrier that shifts from 872 kg at 137.2\$ to 761 kg at 163\$. Even these isolated coordinates successfully illustrate the mathematical conflict between economic and environmental objectives; comparing them to the main Pareto fronts reveals that HO dominates the whole operational area. This shows that while traditional evolutionary frameworks can produce localized trade-offs, they lack the global search capabilities required to escape high-cost, high-emission local minima.

4.3. Convergence Analysis

As shown in Figures 11 and 12, the convergence profiles offer information on the stability, exploration capacity, and quality of solutions attained by each technique across 150 iterations.

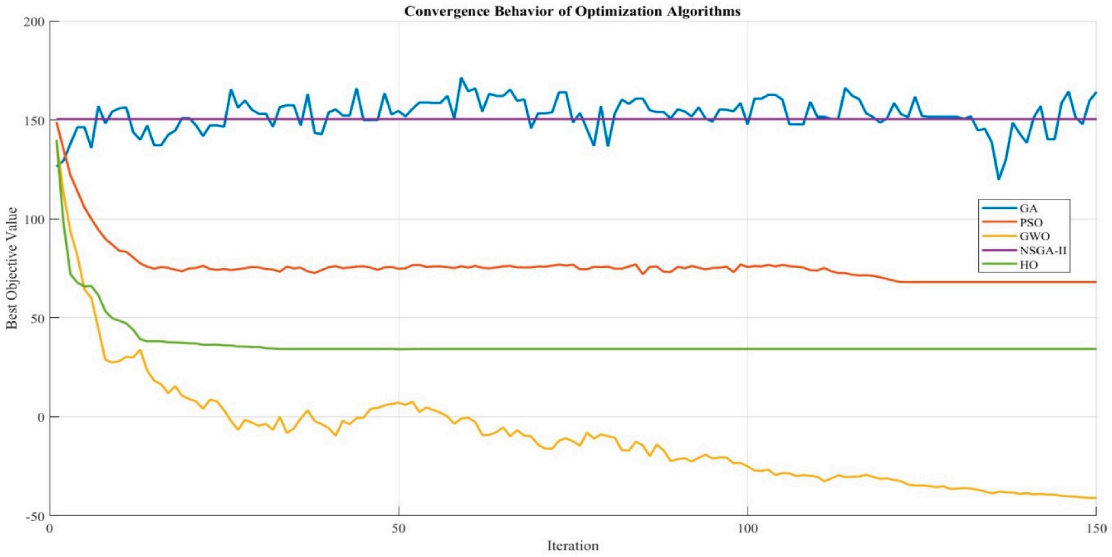


Figure 11. Convergence behavior of the optimization algorithms for Microgrid 1.

This illustrates how each approach minimizes the system's objective across 150 iterations. The convergence history curves for MG1 and MG2 are examined in order to do this. We are able to better understand the trade-offs made according to these curves. The convergence of the HO technique is stable between iterations 25 and 35, and it rapidly levels out and maintains a value

of around 35. This facilitates the HO method's ongoing exploration of many choices, which is necessary given its vast array of possible responses. While GA and NSGA-II remain severely stuck throughout the execution period, swinging inefficiently in the largest sub-optimal value band between 120 and 170, PSO settles into a stable, moderate-cost local optimum near 65 in MG1 and 30 in MG2. However, the GWO technique continues to improve as it descends into the negative region, reaching about −40 by iteration 150. This demonstrates that the GWO approach is less optimal for identifying a wide variety of options.

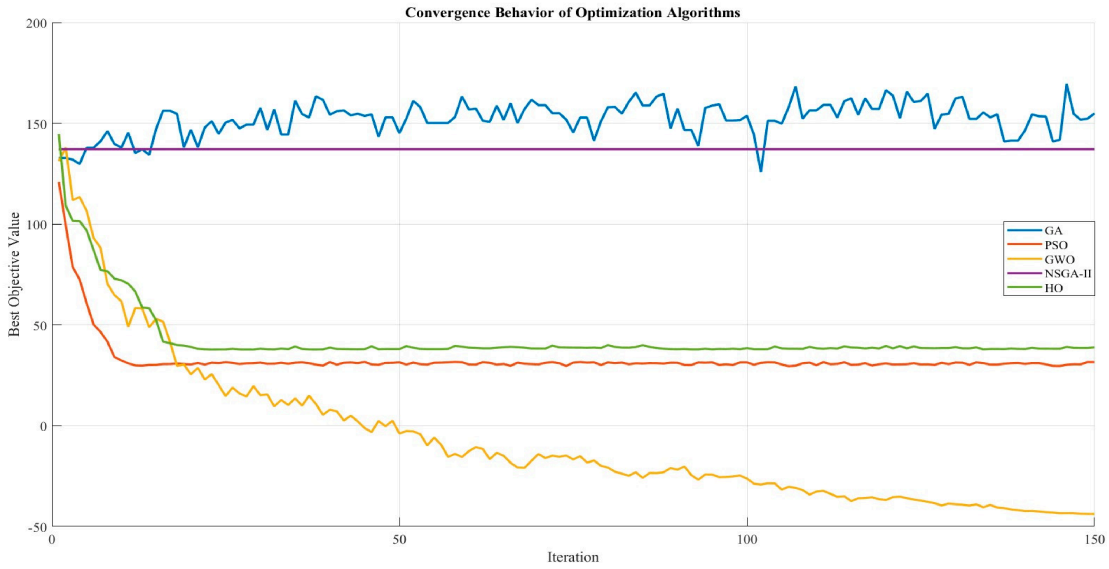


Figure 12. Convergence behavior of the optimization algorithms for Microgrid 2.

4.4. Economic Performance Analysis

Figures 13 and 14 present the statistical distribution of operating costs obtained by different optimization algorithms for MG1 and MG2.

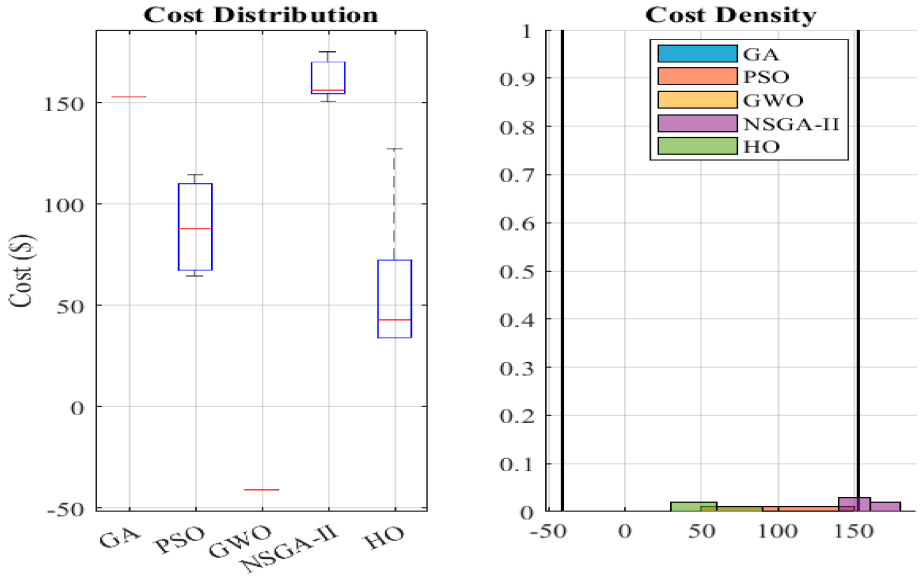


Figure 13. Statistical distribution of operating costs obtained by different optimization algorithms for MG1.

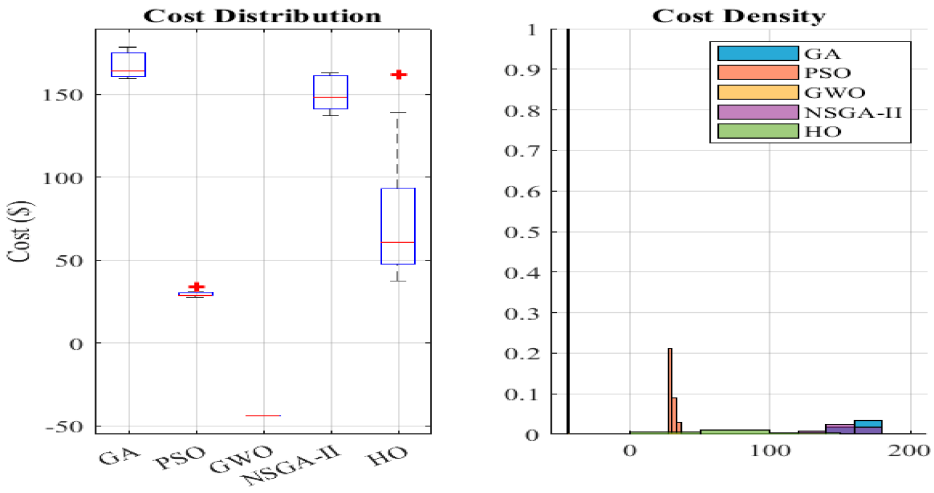


Figure 14. Statistical distribution of operating costs obtained by different optimization algorithms for MG2.

The statistical cost distributions of MG1 and MG2 also emphasize the architectural differences between the algorithms. The Hippopotamus Optimization (HO) has a very balanced search behavior. This is evident from the wide interquartile range from 35$ to 95$ and the smooth and low-density distribution over the favorable cost landscape. In contrast, GWO has zero variance, collapsing completely to a single-point negative-cost spike at −40$. PSO is very accurate locally. PSO is clustered closely around a median of 88$ in MG1 and has a dense and sharp peak around 30$ in MG2. On the other hand, the distributions for GA and NSGA-II are completely constrained within the highest sub-optimal cost bracket, between 140$ and 175$, demonstrating their incapacity to explore more economically feasible microgrid dispatch configurations. This figure illustrates the statistical distribution of operational costs achieved by different EMS optimization algorithms in MG1 and MG2, as shown in Figures 15 and 16.

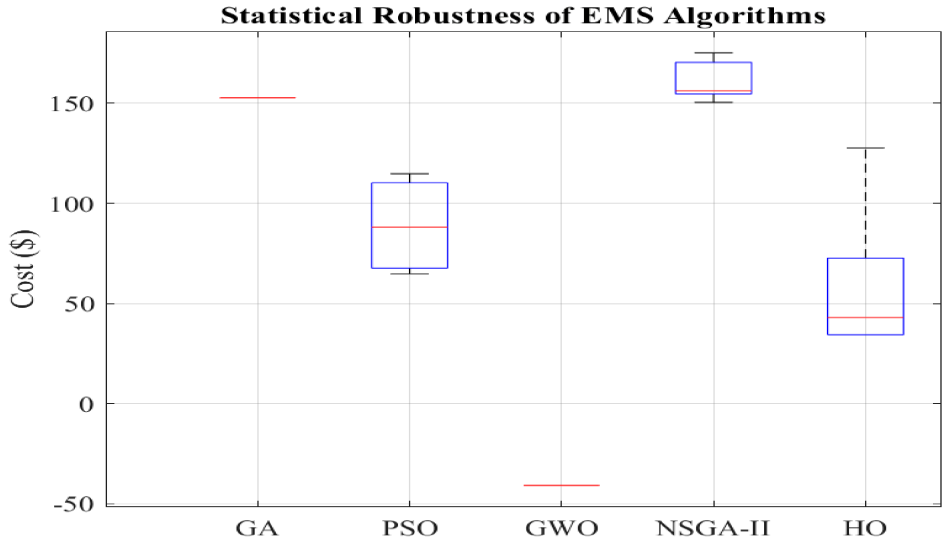


Figure 15. Statistical robustness analysis of EMS algorithms based on operating cost distributions in MG1.

This model uses the operational cost distributions for MG1 and MG2 to assess the statistical robustness of the EMS algorithms. With a well-spread interquartile range (IQR) from $35 to $95, the Hippopotamus Optimization (HO) exhibits high structural robustness and balanced exploration capacity in various Pareto-optimal trade-offs. GWO, on the other

hand, has zero variation and, as a result of severe local exploitation, collapses entirely into a single point negative-cost line, −$40. With tight clustering around a median cost of $88 in MG1 and locking onto an extremely small economic window of $30 in MG2, PSO exhibits remarkable local consistency. On the other hand, because of local minima stagnation, GA and NSGA-II show poor optimization resilience, being entirely contained between the cost limits of 140$ and 175$ (very sub-optimal).

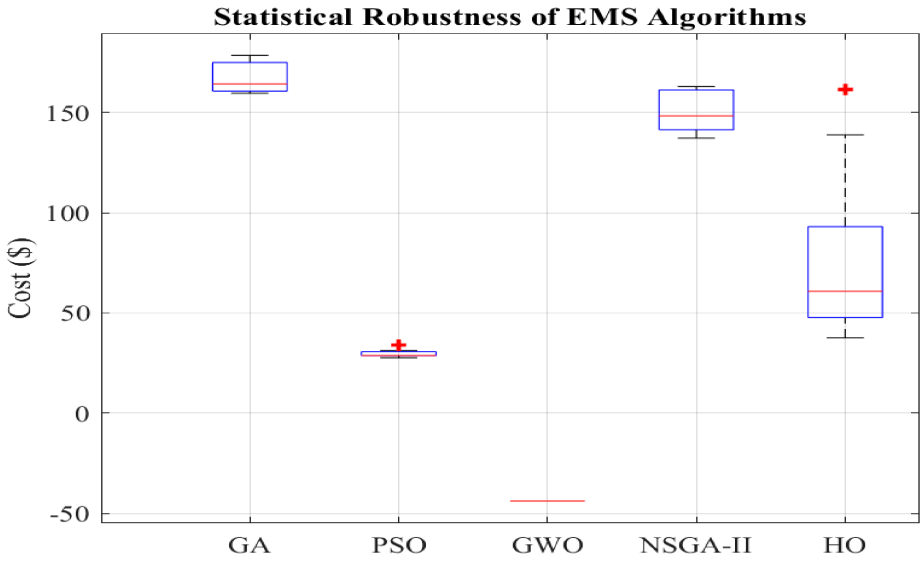


Figure 16. Statistical robustness analysis of EMS algorithms based on operating cost distributions in MG2.

4.5. Energy Dispatch Analysis

The dispatch results demonstrate how the EMS coordinates renewable generation, storage systems, and grid interaction to achieve economically and operationally efficient microgrid performance, as shown in Figures 17 and 18.

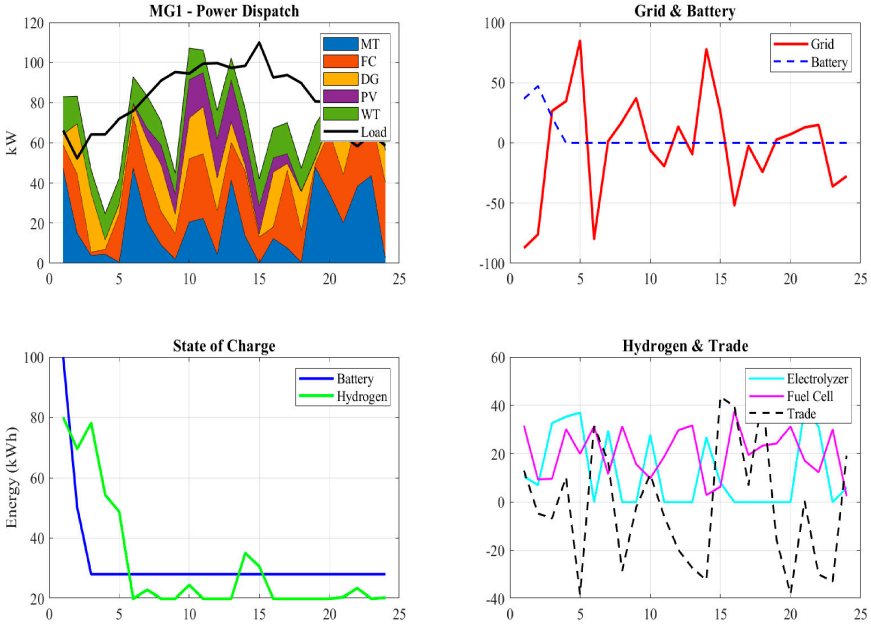


Figure 17. Power dispatch profiles of MG1 under the proposed energy management system (EMS).

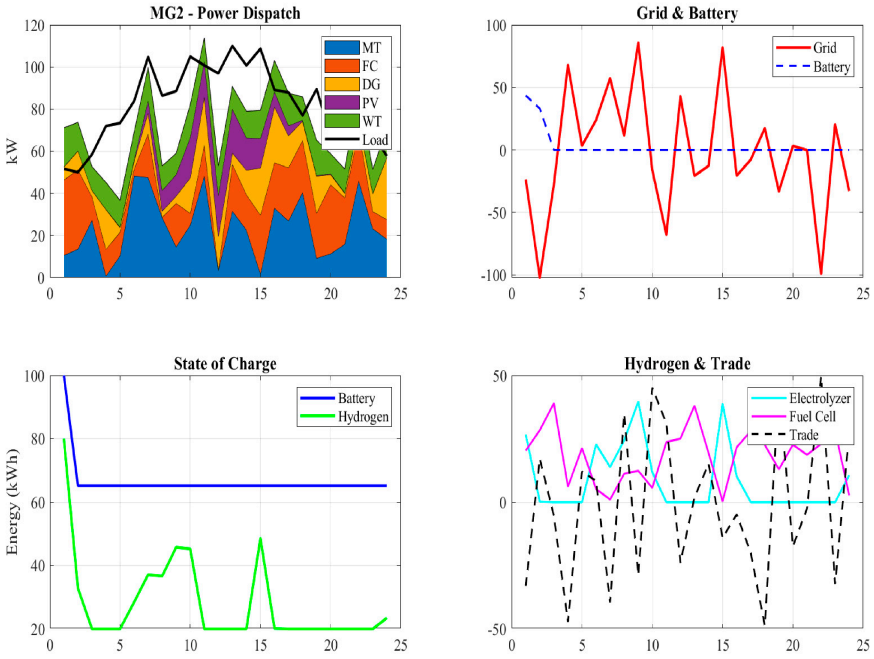


Figure 18. Power dispatch profiles of MG2 under the proposed energy management system (EMS).

Utilizing as much solar and wind energy as feasible is the goal of the energy management system (EMS). Additionally, it takes into account the limitations of battery and hydrogen storage during peak renewable energy hours (5 to 15 h). The significant dips in power returning to the system, down to −100 kW, are indicative of changes in the amounts of electricity the grid exchanges. This significant energy export demonstrates how the EMS employs more clean energy to increase the microgrid's profitability. It also demonstrates the possibility of operational expenses for the microgrid. By using wind energy and sending excess energy back to the grid, the EMS makes the microgrid viable. The EMS maximizes the profitability of microgrids. The microgrid makes extensive use of solar and wind energy. During periods of peak generation, the microgrid exports energy back to the grid. Figures 17 and 18 illustrate the 24 h state of charge (SOC) profiles of the battery and hydrogen storage systems in MG1 and MG2. MG1 and MG2's 24 h energy storage state of charge (SOC) dynamics show that both storages are rapidly depleted in the first three hours to meet the initial demand. Due to system limitations, the battery SOC in MG1 is stabilized at a minimum of 28%, and in MG2 at a higher baseline of 65%. However, the hydrogen SOC curves in both systems are highly adaptable, rising to absorb excess energy during peak renewable-generation windows (hours 6–10 and hour 15) and occasionally falling to the lower bound of 20%. This demonstrates that the EMS respects the operational restrictions of both microgrids while utilizing the flexibility of hydrogen storage to achieve optimal energy arbitrage.

4.6. Statistical Validation, Sensitivity, and Ablation Studies

To meet the demands for reproducibility and robustness in the multi-objective comparative evaluation, this section presents: (i) quantitative hypervolume (HV) measures; (ii) non-parametric testing for statistical significance in terms of independent executions, (iii) sensitivity of the results with respect to the number of uncertainty scenarios and the price of carbon, (iv) a counterfactual quantification of the value of P2P trading, and (v) ablation of the deterministic vs. stochastic formulation.

4.6.1. Hypervolume-Based Quantitative Analysis

To quantify the quality of the Pareto fronts obtained in Figures 7 and 8 beyond visual inspection, the hypervolume (HV) indicator was computed for all five algorithms under two normalization schemes, specifically, (i) per-front normalization (each algorithm normalized to its own min–max range) and (ii) global normalization (a single min–max range shared across all algorithms, with a common reference point of (1.1, 1.1)), the latter being the only scheme suitable for fair cross-algorithm comparison. Table 1 shows hypervolume (HV) outcomes across the five algorithms.

Table 1. Hypervolume (HV) outcomes across the five algorithms.

Algorithm	HV MG1 (Pre-Front)	HV MG1 (Global)	HV MG2 (Pre-Front)	HV MG2 (Global)
GA	0.274082627	0.054493059	0.714595147	0.084525859
PSO	0.537918541	0.341337978	0.526352533	0.511652153
GWO	1.1025	1.1025	1.1025	1.1025
NSGA-II	0.562412494	0.068134512	0.675683952	0.130641734
HO	0.607258637	0.535021844	0.650111066	0.454590004

In terms of global normalization, which is the only metric that is comparable across all algorithms, HO obtains the largest HV for physically meaningful algorithms in both microgrids (0.535 and 0.455), followed by PSO (0.341 and 0.512). The HV values obtained by GA and NSGA-II are noticeably smaller, as indicated in Section 4.3. The GWO score is inflated, since the Pareto front converges to an unrealistic single point lying outside the physically feasible range of trade-off.

4.6.2. Statistical Significance and Computational Efficiency

In order to ensure that the different costs are not due to the seed effects, the algorithms have been independently executed N = 30 times for each microgrid and the Wilcoxon rank-sum test was performed on the cost distribution pairs, as shown in Tables 2 and 3.

Table 2. Wilcoxon rank-sum test *p*-values—MG1.

	GA	PSO	GWO	NSGA-II	HO
GA	1	3.02×10^{-11}	3.02×10^{-11}	2.39×10^{-8}	3.02×10^{-11}
PSO	3.02×10^{-11}	1	3.02×10^{-11}	3.02×10^{-11}	0.411911
GWO	3.02×10^{-11}	3.02×10^{-11}	1	3.02×10^{-11}	3.02×10^{-11}
NSGA-II	2.39×10^{-8}	3.02×10^{-11}	3.02×10^{-11}	1	3.02×10^{-11}
HO	3.02×10^{-11}	0.411911	3.02×10^{-11}	3.02×10^{-11}	1

Table 3. Wilcoxon rank-sum test *p*-values—MG2.

	GA	PSO	GWO	NSGA-II	HO
GA	1	3.02×10^{-11}	3.02×10^{-11}	4.31×10^{-8}	3.02×10^{-11}
PSO	3.02×10^{-11}	1	3.34×10^{-11}	3.02×10^{-11}	0.549327
GWO	3.02×10^{-11}	3.34×10^{-11}	1	3.02×10^{-11}	3.02×10^{-11}
NSGA-II	4.31×10^{-8}	3.02×10^{-11}	3.02×10^{-11}	1	3.02×10^{-11}
HO	3.02×10^{-11}	0.549327	3.02×10^{-11}	3.02×10^{-11}	1

HO demonstrates a statistically significant cost savings when compared with GA and NSGA-II ($p < 10^{-7}$ in both microgrids), whereas no statistical significance is detected when compared with PSO ($p = 0.41$–$0.55 > 0.05$). This means that HO and PSO are statistically

equivalent top-performing solvers in solving this problem. Table 4 shows the computational time analysis per microgrid.

Table 4. Computational time analysis (30 runs per MG).

Algorithm	Mean Time (s)	Std Dev (s)	Min (s)	Max (s)
GA	3.62	0.70	2.7	5.8
PSO	1.64	0.07	1.6	1.9
GWO	2.12	0.10	2.0	2.3
NSGA-II	2.97	0.13	2.8	3.2
HO	1.58	0.06	1.5	1.7

The combination of cost-effectiveness and shortest average time with minimum variation in execution times justifies the applicability of HO in practical scenarios of re-dispatching.

4.6.3. Sensitivity with Regards to Number of Scenarios

To establish the correctness of the results obtained on the N = 10 LHS scenario set used in the main experiments, optimization was conducted for Nsc = {5, 10, 20, 30} scenarios (with the same sets of scenarios for each number considered by each algorithm). Table 5 shows the hypervolume sensitivity of the solution to scenario count.

This approach resulted in the average HV over both microgrids having an interval of 0.67 to 0.74 but no strictly monotonic behavior; in particular, an increase in the scenario count from Nsc = 10 to Nsc = 30 led to the HV MG1 to drop by ≈11% and to the HV MG2 increase by ≈6.5%, leading to a net HV drop by ≈3%.

Table 5. Hypervolume sensitivity of solution to scenario count.

N Scenarios	HV MG1	HV MG2	Average Value of MG1,2
5	0.755589274	0.583130361	0.6694
10	0.821662876	0.651734985	0.7367
20	0.581140808	0.758666696	0.6699
30	0.734057264	0.694089215	0.7141

4.6.4. Sensitivity of the Carbon Price

Since the Pareto fronts for the bi-objective problem (cost, CO_2) are determined independently of carbon prices, a range of carbon prices (0–200 $/t) was used simply as a tool to choose a knee point on the fixed front. Table 6 shows the sensitivity of carbon price on selected compromise solutions.

Table 6. Sensitivity of carbon price on selected compromise solutions.

Carbon Price ($/t)	Cost MG1 ($)	CO_2 MG1 (kg)	Cost MG2 ($)	CO_2 MG2 (kg)
0	147.69	909.89	140.60	856.25
25	152.83	748.97	189.30	787.26
50–200	152.83	748.97	189.30	787.26

There is a dramatic change from $0/t to $25/t (carbon dioxide reduction of 17.7% for MG1 and 8.1% for MG2, with respect to marginal cost) after which there is a saturation at the chosen point up to $200/t. The saturation in question is only due to the present density of the Pareto front under consideration and does not imply any economic indifference at all.

4.6.5. Estimation of the Economic and Environmental Value of P2P Trade

In order to obtain the total impact of inter-microgrid P2P trading, which is a decision variable of the EMS but not considered in isolation in the original results, we optimized each algorithm under two scenarios: (i) the baseline case where trading is allowed, and (ii) an alternate scenario where trading is prohibited (Trade. Pmax = 0), as shown in Figure 19.

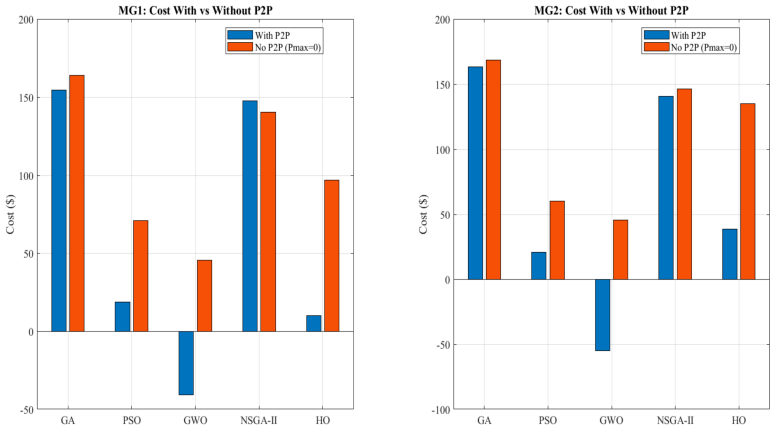


Figure 19. Effect of peer-to-peer trading—MG1 and MG2.

Operating cost is always reduced (between 3% to 90%, based on algorithm used), but at the same time, CO_2 emission is always increased in most cases. This conforms to the basic trade-off between cost and emission as illustrated in Figures 9 and 10, where any solution with lower cost and hence greater economic flexibility through exporting/importing of economic goods must always be with higher dispatch emissions. P2P trading thus serves only as a mechanism of economic flexibility.

4.6.6. Value of Stochastic Solution: Deterministic Ablation vs. Stochastic Ablation

In order to identify the specific effect of the stochastic approach compared to that of the deterministic approach, both methods were carried out independently N = 10 times for each microgrid, where the deterministic solution was tested out-of-sample (OOS) on all scenarios, as shown in Figure 20.

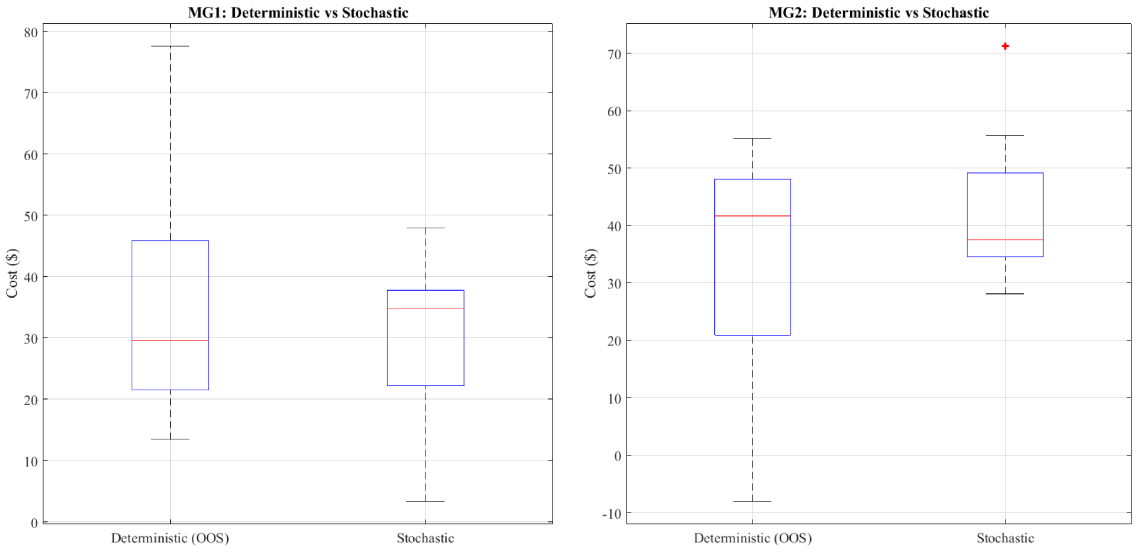


Figure 20. Cost distribution: deterministic (OOS) v. stochastic (N = 10 trials).

The deterministic approach sometimes results in a slightly better median cost but has much greater tail risk, with a tail risk value of $77 for MG1 and a negative cost for MG2, which is inconsistent with economics. The stochastic solution, on the other hand, has a consistently smaller interquartile range (by 33–45%) and does not exhibit negative cost at all. This clearly demonstrates that the main advantage of the stochastic solution is its lower dispersion, and not the minimization of cost, which is the essence of stochastic programming.

5. Conclusions

In the current study, a stochastic bi-objective EMS model was developed to evaluate the performance of hybrid battery–hydrogen microgrids in the face of renewable uncertainties. Five different algorithms, such as HO, PSO, GWO, GA, and NSGA-II, were evaluated on two different designs of microgrids. Hypervolume-based analysis showed that HO obtained the best hypervolume value compared to other physically valid solutions (0.535/0.455 for MG1/MG2), followed by PSO. On the contrary, the solutions obtained using GA and NSGA-II were stuck in a sub-optimal solution area ($137–$175). Wilcoxon rank-sum test results on 30 random runs revealed HO's superiority over GA/NSGA-II (p-value $< 10^{-7}$) but no significant difference between HO and PSO (p-value ~0.41–0.55). The GWO score is inflated, since the Pareto front converges to an unrealistic single point lying outside the physically feasible range of trade-off. The counterfactual analysis of P2P trading for all algorithms revealed that while trading decreases the cost (by 3–90%), it generally leads to higher emissions, indicating that trading simply shifts the operating point on the cost–emissions frontier rather than decreasing emissions. Consequently, trading should be considered in future optimizations through incorporation of trading costs directly. Comparing the ablation formulation to the deterministic approach revealed that while mean costs were similar, the stochastic formulation led to a 33–45% narrower interquartile range of costs. The results from the sensitivity analysis reveal non-linear HV values depending on the number of scenarios (Nsc $\in \{5, 10, 20, 30\}$), and hence recommend 10 as a good option, while further revealing that the effect of carbon pricing is limited to the selected knee-point solution only at low prices ($0–$25/t), but did not change the algorithm rankings. On an operational basis, the model used in the optimization of the EMS successfully scheduled the allocation of renewable energy surpluses to the storage of batteries/hydrogen and grid transactions, as seen in the 24 h scheduling chart. This research still serves as an experiment in simulation feasibility; hardware-in-the-loop (HIL) testing with real storage units is considered an important next step. The stochastic formulation was limited to uncertainty on the renewable-generation side (supported by the LSTM forecast error analysis: 18.4% RMSE for PV and 2.3% for WT); it would be valuable to include uncertainty on the load and price side and run the scenario count sensitivity with different seeds and algorithms, as well as conduct sensitivity studies for the storage capacity and algorithm hyperparameters (electrolyzer/fuel cell degradation).

Author Contributions: E.I.E.-S. and S.K.E.: Conceptualization, Methodology, Software, Visualization, Project administration, Investigation, Formal analysis, Writing—Original draft preparation, Writing—Review and Editing. A.A.F.Y., I.B., F.H.A. and A.M.E.-R.: Data curation, Validation, Supervision, Resources, Writing—Review and Editing, Project administration, Funding Acquisition. All authors have read and agreed to the published version of the manuscript.

Funding: This work is funded and supported by the Deanship of Graduate Studies and Scientific Research, Taif University.

Institutional Review Board Statement: Not applicable.

Informed Consent Statement: Not applicable.

Data Availability Statement: The raw data supporting the conclusions of this article will be made available by the authors on request.

Acknowledgments: The authors would like to acknowledge the Deanship of Graduate Studies and Scientific Research, Taif University for technically supporting this work.

Conflicts of Interest: The authors declare no conflicts of interest.

References

1. Paul, K.; Jyothi, B.; Kumar, R.S.; Singh, A.R.; Bajaj, M.; Kumar, B.H.; Zaitsev, I. Optimizing sustainable energy management in grid connected microgrids using quantum particle swarm optimization for cost and emission reduction. *Sci. Rep.* **2025**, *15*, 5843. [CrossRef] [PubMed]
2. Singh, A.R.; Kumar, R.S.; Bajaj, M.; Khadse, C.B.; Zaitsev, I. Machine learning-based energy management and power forecasting in grid-connected microgrids with multiple distributed energy sources. *Sci. Rep.* **2024**, *14*, 19207. [CrossRef] [PubMed]
3. Moosavi, M.; Olamaei, J.; Shourkaei, H.M. Optimizing microgrid performance a multi-objective strategy for integrated energy management with hybrid sources and demand response. *Sci. Rep.* **2025**, *15*, 17827. [CrossRef] [PubMed]
4. Saravanakumar, V.; Vijayalakshmi, V. Microgrid Management of Hybrid Energy Sources Using a Hybrid Optimization Algorithm. *Energy Storage* **2025**, *7*, e70070. [CrossRef]
5. Roslan, M.F.; Hannan, M.; Ker, P.J.; Begum, R.; Mahlia, T.I.; Dong, Z. Scheduling controller for microgrids energy management system using optimization algorithm in achieving cost saving and emission reduction. *Appl. Energy* **2021**, *292*, 116883. [CrossRef]
6. Alkuhayli, A.; Dashtdar, M.; Flah, A.; El-Bayeh, C.Z.; Blazek, V.; Prokop, L. Designing a multi-objective energy management system in multiple interconnected water and power microgrids based on the MOPSO algorithm. *Heliyon* **2024**, *10*, e31280. [CrossRef] [PubMed]
7. Neelashetty, K.; Kumara, V.P.; Sharma, P.V.R.; Pramod; Krishna, V.B.M. Two-Stage Stochastic Optimization for Cost-Effective Energy Management in Grid-tied Microgrids. *Int. J. Comput. Exp. Sci. Eng.* **2025**, *11*, 998–1003. [CrossRef]
8. Wang, B.; Zhang, C.; Dong, Z.Y. Interval Optimization Based Coordination of Demand Response and Battery Energy Storage System Considering SOC Management in a Microgrid. *IEEE Trans. Sustain. Energy* **2020**, *11*, 2922–2931. [CrossRef]
9. Seyedeh-Barhagh, S.; Abapour, M.; Mohammadi-Ivatloo, B.; Shafie-Khah, M.; Laaksonen, H. Optimal scheduling of a microgrid based on renewable resources and demand response program using stochastic and IGDT-based approach. *J. Energy Storage* **2024**, *86*, 111306. [CrossRef]
10. Bhatia, A.A.; Das, D. Demand response strategy for microgrid energy management integrating electric vehicles, battery energy storage system, and distributed generators considering uncertainties. *Sustain. Energy Grids Netw.* **2024**, *41*, 101594. [CrossRef]
11. Dey, B.; Misra, S.; Marquez, F.P.G. Microgrid system energy management with demand response program for clean and economical operation. *Appl. Energy* **2023**, *334*, 120717. [CrossRef]
12. Dey, B.; Basak, S.; Bhattacharyya, B. Demand-Side-Management-Based Bi-level Intelligent Optimal Approach for Cost-Centric Energy Management of a Microgrid System. *Arab. J. Sci. Eng.* **2023**, *48*, 6819–6830. [CrossRef]
13. Ba-Swaimi, S.; Verayiah, R.; Ramachandaramurthy, V.K.; Alahmad, A.K. Long-term optimal planning of distributed generations and battery energy storage systems towards high integration of green energy considering uncertainty and demand response program. *J. Energy Storage* **2024**, *100*, 113562. [CrossRef]
14. Ba-Swaimi, S.; Verayiah, R.; Ramachandaramurthy, V.K.; Alahmad, A.K.; Padmanaban, S. Optimal Planning of Renewable Distributed Generators and Battery Energy Storage Systems in Reconfigurable Distribution Systems with Demand Response Program to Enhance Renewable Energy Penetration. *Results Eng.* **2025**, *25*, 104304. [CrossRef]
15. Khasanov, M.; Kamel, S.; Rahmann, C.; Hasanien, H.M.; Al-Durra, A. Optimal distributed generation and battery energy storage units integration in distribution systems considering power generation uncertainty. *IET Gener. Transm. Distrib.* **2021**, *15*, 3400–3422. [CrossRef]
16. Aryanezhad, M. A robust game-theoretic optimization model for battery energy storage in multi-microgrids by considering of renewable based DGs uncertainty. *Electr. Power Syst. Res.* **2022**, *204*, 107591. [CrossRef]
17. Atiea, M.A.; El-Rifaie, A.M.; Moustafa, G.; Shaheen, A.M. A scalable forecasting framework for PV systems using hyper-tuned regressors and environmental data. *Unconv. Resour.* **2025**, *8*, 100236. [CrossRef]
18. Merabet, A.; Al-Durra, A.; El-Saadany, E.F. Energy management system for optimal cost and storage utilization of renewable hybrid energy microgrid. *Energy Convers. Manag.* **2022**, *252*, 115116. [CrossRef]
19. Luo, L.; Abdulkareem, S.S.; Rezvani, A.; Miveh, M.R.; Samad, S.; Aljojo, N.; Pazhoohesh, M. Optimal scheduling of a renewable based microgrid considering photovoltaic system and battery energy storage under uncertainty. *J. Energy Storage* **2020**, *28*, 101306. [CrossRef]

20. Ramkumar, M.; Subramani, J.; Sivaramkrishnan, M.; Munimathan, A.; Michael, G.K.O.; Alam, M.M. Optimal energy management for multi-energy microgrids using hybrid solutions to address renewable energy source uncertainty. *Sci. Rep.* **2025**, *15*, 7755. [CrossRef] [PubMed]
21. Song, T.; Teh, J. Coordinated Integration of Wind Energy in Microgrids: A Dual Strategy Approach Leveraging Dynamic Thermal Line Rating and Electric Vehicle Scheduling. *Sustain. Energy Grids Netw.* **2024**, *38*, 101299. [CrossRef]
22. Allwyn, R.G.; Margaret, V.; Al-Hinai, A. Microgrid Energy Management—An Optimization Approach for Operational Cost Reduction. In *Proceedings of the 2025 IEEE International Conference on Emerging Trends in Engineering and Computing (ETECOM)*; IEEE: New York, NY, USA, 2025; pp. 1–8. [CrossRef]
23. Labra-Cáceres, N.I.; Grisales-Noreña, L.F.; Bolaños, R.I.; Guzmán-Henao, J.A.; Montoya, O.D. Energy management system for PV-based distributed generators in AC microgrids using an adapted JAYA optimizer to minimize operational costs, energy losses, and CO_2 emissions. *Results Eng.* **2025**, *25*, 104397. [CrossRef]
24. Kassab, F.A.; Celik, B.; Locment, F.; Sechilariu, M.; Liaquat, S.; Hansen, T.M. Optimal sizing and energy management of a microgrid: A joint MILP approach for minimization of energy cost and carbon emission. *Renew. Energy* **2024**, *224*, 120186. [CrossRef]
25. Jasim, A.M.; Jasim, B.H.; Baiceanu, F.-C.; Neagu, B.-C. Optimized Sizing of Energy Management System for Off-Grid Hybrid Solar/Wind/Battery/Biogasifier/Diesel Microgrid System. *Mathematics* **2023**, *11*, 1248. [CrossRef]
26. Samy, M.; Güven, A.F. Optimal dimensioning of grid-connected PV/wind hybrid renewable energy systems with battery and supercapacitor storage a statistical validation of meta-heuristic algorithm performance. *Sci. Rep.* **2025**, *15*, 45658. [CrossRef] [PubMed]
27. Habibi, S.; Effatnejad, R.; Hedayati, M.; Hajihosseini, P. Stochastic energy management of a microgrid incorporating two-point estimation method, mobile storage, and fuzzy multi-objective enhanced grey wolf optimizer. *Sci. Rep.* **2024**, *14*, 1667. [CrossRef] [PubMed]
28. Khawaja, Y.; Qiqieh, I.; Alzubi, J.; Alzubi, O.; Allahham, A.; Giaouris, D. Design of cost-based sizing and energy management framework for standalone microgrid using reinforcement learning. *Sol. Energy* **2023**, *251*, 249–260. [CrossRef]
29. Shayeghi, H.; Davoudkhani, I.F. Uncertainty aware energy management in microgrids with integrated electric bicycle charging stations and green certificate market. *Sci. Rep.* **2025**, *15*, 26374. [CrossRef] [PubMed]
30. Ibrahim, I.M.; Abdelaziz, A.Y.; Alhelou, H.H.; Omran, W.A. Sizing of Microgrid System Including Multi-Functional Battery Storage and Considering Uncertainties. *IEEE Access* **2023**, *11*, 29521–29540. [CrossRef]
31. Gbadega, P.; Balogun, O. Transactive Energy Management for Efficient Scheduling and Storage Utilization in a Grid-connected Renewable Energy-based Microgrid. *E-Prime-Adv. Electr. Eng. Electron. Energy* **2025**, *11*, 100914. [CrossRef]
32. Gugulothu, R.; Nagu, B.; Pullaguram, D. Energy management strategy for standalone DC microgrid system with photovoltaic/fuel cell/battery storage. *J. Energy Storage* **2023**, *57*, 106274. [CrossRef]
33. Obukhov, S.; Ibrahim, A.; Tolba, M.A.; El-Rifaie, A.M. Power Balance Management of an Autonomous Hybrid Energy System Based on the Dual-Energy Storage. *Energies* **2019**, *12*, 4690. [CrossRef]
34. Qi, N.; Huang, K.; Fan, Z.; Xu, B. Long-Term Energy Management for Microgrid with Hybrid Hydrogen-Battery Energy Storage: A Prediction-Free Coordinated Optimization Framework. *Appl. Energy* **2025**, *377*, 124485. [CrossRef]
35. Khan, A.; Bressel, M.; Abbes, D.; Davigny, A.; Bouamama, B.O. Green Energy Integration: Modeling Photovoltaic, Hydrogen, and Battery Systems for Cost and Carbon Emission Reduction in Micro-Grids. In *Proceedings of the 2024 12th International Conference on Systems and Control (ICSC)*; IEEE: New York, NY, USA, 2024; pp. 295–300. [CrossRef]
36. Boujelbene, M.; Basem, A.; Sawwan, H.; Samad, S.; Ben Hamida, M.B.; Amari, A.; Makharov, K.; Safarova, L.; Mahariq, I. Multi-objective optimization of a biogas-fueled multigeneration system with a supercritical CO_2-based power and multi-level cooling cycle: A hybrid ANN-MOPSO approach. *Fuel* **2025**, *405*, 136687. [CrossRef]
37. Rajagopalan, A.; Nagarajan, K.; Bajaj, M.; Uthayakumar, S.; Prokop, L.; Blazek, V. Multi-objective energy management in a renewable and EV-integrated microgrid using an iterative map-based self-adaptive crystal structure algorithm. *Sci. Rep.* **2024**, *14*, 15652. [CrossRef] [PubMed]
38. Akarne, Y.; Essadki, A.; Nasser, T.; Annoukoubi, M. Enhanced Smart Microgrid Scheduling: An empirical study on simultaneous energy supply and demand optimization using binary sparrow search algorithm. *Results Eng.* **2025**, *27*, 106811. [CrossRef]
39. Michael, N.E.; Bansal, R.C.; Ismail, A.A.; Elnady, A.; Hasan, S. Optimized energy management for photovoltaic/wind hybrid micro-grid using energy storage solution. *Int. J. Model. Simul.* **2023**, *45*, 1091–1108. [CrossRef]
40. Yan, H.; Lin, X.; Li, R. Spatiotemporal Coordinated Control Strategy for Grid-Connected Microgrids with Multi-Source Renewable Energy Forecasting and Adaptive Battery Management. In *Proceedings of the 2026 5th International Conference on Smart Grid and Green Energy (ICSGGE)*; IEEE: New York, NY, USA, 2026; pp. 920–924. [CrossRef]
41. Khan, W.; Renhai, F.; Aziz, A.; Yousaf, M.Z.; Cai, Z.; Iqbal, M.U.; Wang, J.; Abdullah, M.; Geremew, M.S. Deep reinforcement learning-based energy management for design and control of off-grid renewable microgrids with dual-battery storage. *Energy Explor. Exploit.* **2025**, *44*, 821–869. [CrossRef]

42. Altimania, M.; Basem, A.; Saydullaev, B.; Atamuratova, Z.; Madaminov, B.; Umarov, A.; Benti, N.E.; Chaka, M.D. Adaptive multi-objective optimization of microgrid energy management using deep reinforcement learning considering battery degradation and renewable uncertainty. *Sci. Rep.* **2026**, *16*, 14296. [CrossRef] [PubMed]
43. Abdolahzadeh, A.; Hassannia, A.; Mousavizadeh, F.; Askari, M.T. Multi-objective stochastic model optimal operation of smart microgrids coalition with penetration renewable energy resources with demand responses. *Sci. Rep.* **2025**, *15*, 22443. [CrossRef] [PubMed]
44. Barbosa, A.M.; Junior, P.R.; Peruchi, R.S.; Rocha, L.C.S.; Pires, A.L.G.; Janda, K. Stochastic multi-objective optimization of hybrid distributed power generation with battery storage systems. *Energy Sources Part B Econ. Plan. Policy* **2025**, *20*, 2504487. [CrossRef]
45. Fathy, A.; Kaaniche, K.; Alanazi, T.M. Recent Approach Based Social Spider Optimizer for Optimal Sizing of Hybrid PV/Wind/Battery/Diesel Integrated Microgrid in Aljouf Region. *IEEE Access* **2020**, *8*, 57630–57645. [CrossRef]
46. Marzband, M.; Ghadimi, M.; Sumper, A.; Domínguez-García, J.L. Experimental Validation of a Real-Time Energy Management System Using Multi-Period Gravitational Search Algorithm for Microgrids in Islanded Mode. *Appl. Energy* **2014**, *128*, 164–174. [CrossRef]
47. Adefarati, T.; Bansal, R.C. Optimal Sizing of Battery Energy Storage in a Microgrid Considering Capacity Degradation and Replacement Year. *Electr. Power Syst. Res.* **2021**, *195*, 107099. [CrossRef]
48. Shi, W.; Li, N.; Chu, C.-C.; Gadh, R. Real-Time Energy Management in Microgrids. *IEEE Trans. Smart Grid.* **2015**, *8*, 228–238. [CrossRef]
49. Tant, J.; Geth, F.; Six, D.; Tant, P.; Driesen, J. Multiobjective Battery Storage to Improve PV Integration in Residential Distribution Grids. *IEEE Trans. Sustain. Energy* **2013**, *4*, 182–191. [CrossRef]
50. Liu, J.; Xu, Z.; Wu, J.; Liu, K.; Guan, X. Optimal planning of distributed hydrogen-based multi-energy systems. *Appl. Energy* **2021**, *281*, 116107. [CrossRef]
51. Cano, A.; Jurado, F.; Sanchez, H.; Fernandez, L.M.; Castañeda, M. Optimal Sizing of Stand-Alone Hybrid Systems Based on PV/WT/FC by Using Several Methodologies. *J. Energy Inst.* **2014**, *87*, 330–340. [CrossRef]
52. European Environment Agency (EEA). Greenhouse Gas Emission Intensity of Electricity Generation in Europe. EEA Indicator: Copenhagen, Denmark, 2024. Available online: https://www.eea.europa.eu/en/analysis/indicators/greenhouse-gas-emission-intensity-of-1 (accessed on 2 August 2026).
53. PwC France. *European Carbon Factor 2025*; PricewaterhouseCoopers: Paris, France, 2025; Available online: https://www.pwc.fr/en/publications/series/carbon-factor.html (accessed on 2 August 2026).
54. European Securities and Markets Authority (ESMA). *EU Carbon Markets Report 2025*; ESMA: Paris, France, 2025. Available online: https://www.esma.europa.eu (accessed on 2 August 2026).
55. Wei, X.; Liu, J.; Xu, Y.; Sun, H. Virtual Power Plants Peer-to-Peer Energy Trading in Unbalanced Distribution Networks: A Distributed Robust Approach Against Communication Failures. *IEEE Trans. Smart Grid* **2024**, *15*, 2017–2029. [CrossRef]
56. Wang, H.; Huang, J.W. Incentivizing Energy Trading for Interconnected Microgrids. *IEEE Trans. Smart Grid* **2018**, *9*, 2647–2657. [CrossRef]
57. Radosavljević, J. *Metaheuristic Optimization in Power Engineering*; The Institution of Engineering and Technology (IET): London, UK, 2018.
58. Husein, M.; Chung, I.-Y. Day-Ahead Solar Irradiance Forecasting for Microgrids Using a Long Short-Term Memory Recurrent Neural Network: A Deep Learning Approach. *Energies* **2019**, *12*, 1856. [CrossRef]
59. El-Sayed, E.I.; ElSayed, S.K.; Alsharef, M. Data-Driven Approaches for State-of-Charge Estimation in Battery Electric Vehicles Using Machine and Deep Learning Techniques. *Sustainability* **2024**, *16*, 9301. [CrossRef]
60. Singh, S.; Subburaj, V.; Sivakumar, K.; Kumar, R.A.; Muthuramam, M.S.; Rastogi, R.; Patil, V.R.; Rajaram, A. Optimum Power Forecasting Technique for Hybrid Renewable Energy Systems Using Deep Learning. *Electr. Power Compon. Syst.* **2024**, *53*, 782–799. [CrossRef]
61. Gao, S.; Wang, Y.; Zhou, Y.; Yu, H. An Improved Scheduling Approach for Multi-Energy Microgrids Considering Scenario Insufficiency and Computational Complexity. *Processes* **2025**, *13*, 576. [CrossRef]
62. Wang, G.; Su, T. Uncertainty Quantification for the Impact of Clustered EVs on Microgrid Scheduling Using Latin Hypercube Sampling. In *Proceedings of the 2025 IEEE 9th Conference on Energy Internet and Energy System Integration (EI2)*; IEEE: New York, NY, USA, 2025; pp. 238–244. [CrossRef]
63. Khajuria, R.; Lamba, R.; Kumar, R. A Multi-Objective Approach for Energy Management of Data Center Microgrid Considering Carbon Emission and Operational Cost. In *Proceedings of the 2024 IEEE International Conference on Power Electronics, Drives and Energy Systems (PEDES)*; IEEE: New York, NY, USA, 2024; pp. 1–6. [CrossRef]
64. Suresh, V.; Janik, P.; Jasinski, M.; Guerrero, J.M.; Leonowicz, Z. Microgrid energy management using metaheuristic optimization algorithms. *Appl. Soft Comput.* **2022**, *134*, 109981. [CrossRef]
65. Fathy, A.; Rezk, H.; Ferahtia, S.; Ghoniem, R.M.; Alkanhel, R. An efficient honey badger algorithm for scheduling the microgrid energy management. *Energy Rep.* **2023**, *9*, 2058–2074. [CrossRef]

66. Vásquez, L.P.O.; Redondo, J.L.; Hervás, J.D.Á.; Ramírez, V.M.; Torres, J.L. Balancing CO_2 emissions and economic cost in a microgrid through an energy management system using MPC and multi-objective optimization. *Appl. Energy* **2023**, *347*, 120998. [CrossRef]
67. Mayer, M.J.; Szilágyi, A.; Gróf, G. Environmental and economic multi-objective optimization of a household level hybrid renewable energy system by genetic algorithm. *Appl. Energy* **2020**, *269*, 115058. [CrossRef]
68. Chakraborty, A.; Ray, S. Economic and environmental factors based multi-objective approach for optimizing energy management in a microgrid. *Renew. Energy* **2024**, *222*, 119920. [CrossRef]
69. Li, J.; Li, G.; Ma, S.; Liang, Z.; Li, Y.; Zeng, W. Modeling and Simulation of Hydrogen Energy Storage System for Power-to-gas and Gas-to-power Systems. *J. Mod. Power Syst. Clean Energy* **2023**, *11*, 885–895. [CrossRef]
70. ElSayed, S.K.; Issa, E. Techno-economic optimization for sustainable and efficient green hydrogen export. *Clean Energy* **2025**, *9*, 109–120. [CrossRef]
71. da Silva, G.A.; Aage, N.; Beck, A.T.; Sigmund, O. Local versus global stress constraint strategies in topology optimization: A comparative study. *Int. J. Numer. Methods Eng.* **2021**, *122*, 6003–6036. [CrossRef]
72. Vega, H.P.; Grisales-Noreña, L.F.; Botero-Gómez, V. Optimizing Energy Management in AC Microgrids: A Comparative Study of Metaheuristic Algorithms for Minimizing Energy Losses and CO_2 Emissions. *Stat. Optim. Inf. Comput.* **2025**, *14*, 636–662. [CrossRef]
73. Mahdi, B.S.; Sulaiman, N.; Shehab, M.A.; Shafie, S.; Hizam, H.; Hassan, S.L.B.M. Optimization of Operating Cost and Energy Consumption in a Smart Grid. *IEEE Access* **2024**, *12*, 18837–18850. [CrossRef]
74. Mathur, A.; Kumari, R.; Meena, V.P.; Singh, V.P.; Azar, A.T.; Hameed, I.A. Data-driven optimization for microgrid control under distributed energy resource variability. *Sci. Rep.* **2024**, *14*, 10806. [CrossRef] [PubMed]
75. Mars, N.; Houcine, L.; Chaabani, M.; Zaafouri, A. Hippopotamus algorithm for optimal sizing of hybrid renewable energy system. *Results Eng.* **2026**, *29*, 109772. [CrossRef]

Disclaimer/Publisher's Note: The statements, opinions and data contained in all publications are solely those of the individual author(s) and contributor(s) and not of MDPI and/or the editor(s). MDPI and/or the editor(s) disclaim responsibility for any injury to people or property resulting from any ideas, methods, instructions or products referred to in the content.